

# On scenarios of the onset of homoclinic attractors in three-dimensional non-orientable maps

Cite as: Chaos **31**, 043122 (2021); <https://doi.org/10.1063/5.0039870>

Submitted: 07 December 2020 • Accepted: 25 March 2021 • Published Online: 15 April 2021

 A. S. Gonchenko,  M. S. Gonchenko,  A. D. Kozlov, et al.

## COLLECTIONS

Paper published as part of the special topic on [Global Bifurcations, Chaos, and Hyperchaos: Theory and Applications](#)



View Online



Export Citation



CrossMark

## ARTICLES YOU MAY BE INTERESTED IN

### [On discrete Lorenz-like attractors](#)

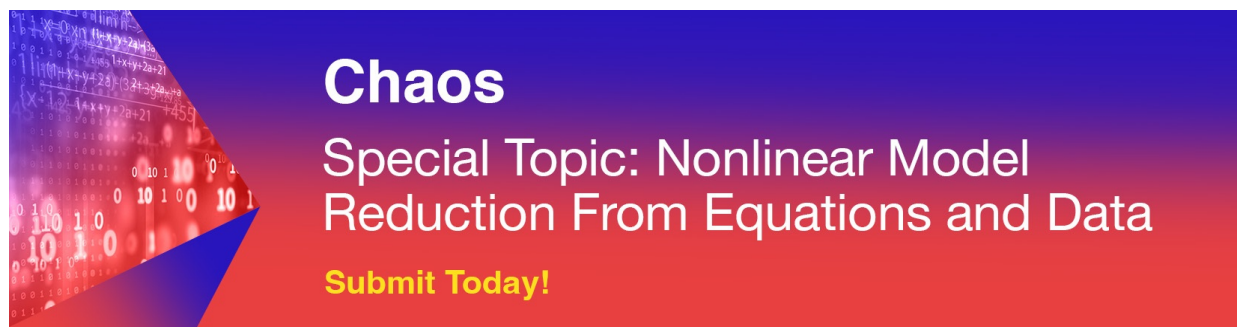
Chaos: An Interdisciplinary Journal of Nonlinear Science **31**, 023117 (2021); <https://doi.org/10.1063/5.0037621>

### [Shilnikov attractors in three-dimensional orientation-reversing maps](#)

Chaos: An Interdisciplinary Journal of Nonlinear Science **31**, 011102 (2021); <https://doi.org/10.1063/5.0036405>

### [A criterion for mixed dynamics in two-dimensional reversible maps](#)

Chaos: An Interdisciplinary Journal of Nonlinear Science **31**, 043133 (2021); <https://doi.org/10.1063/5.0040444>



**Chaos**  
Special Topic: Nonlinear Model  
Reduction From Equations and Data  
**Submit Today!**

# On scenarios of the onset of homoclinic attractors in three-dimensional non-orientable maps

Cite as: Chaos 31, 043122 (2021); doi: 10.1063/5.0039870

Submitted: 7 December 2020 · Accepted: 25 March 2021 ·

Published Online: 15 April 2021



View Online



Export Citation



CrossMark

A. S. Gonchenko,<sup>1,2,a)</sup> M. S. Gonchenko,<sup>3,b)</sup> A. D. Kozlov,<sup>1,c)</sup> and E. A. Samylina<sup>2,d)</sup>

## AFFILIATIONS

<sup>1</sup>Scientific and Educational Mathematical Center “Mathematics of Future Technologies,” Lobachevsky State University of Nizhny Novgorod, 23 Gagarina Ave., 603950 Nizhny Novgorod, Russia

<sup>2</sup>National Research University Higher School of Economics, 25/12 Bolshaya Pecherskaya Ulitsa, 603155 Nizhny Novgorod, Russia

<sup>3</sup>Departament de Matemàtiques, Universitat Politècnica de Catalunya, Av. Diagonal 647, 08028 Barcelona, Spain

**Note:** This paper is part of the Focus Issue, Global Bifurcations, Chaos, and Hyperchaos: Theory and Applications.

<sup>a)</sup>Electronic mail: [agonchenko@mail.ru](mailto:agonchenko@mail.ru)

<sup>b)</sup>Author to whom correspondence should be addressed: [marina.gonchenko@upc.edu](mailto:marina.gonchenko@upc.edu)

<sup>c)</sup>Electronic mail: [kozloff@list.ru](mailto:kozloff@list.ru)

<sup>d)</sup>Electronic mail: [samylina\\_evgeniya@mail.ru](mailto:samylina_evgeniya@mail.ru)

## ABSTRACT

We study scenarios of the appearance of strange homoclinic attractors (which contain only one fixed point of saddle type) for one-parameter families of three-dimensional non-orientable maps. We describe several types of such scenarios that lead to the appearance of discrete homoclinic attractors including Lorenz-like and figure-8 attractors (which contain a saddle fixed point) as well as two types of attractors of spiral chaos (which contain saddle-focus fixed points with the one-dimensional and two-dimensional unstable manifolds, respectively). We also emphasize peculiarities of the scenarios and compare them with the known scenarios in the orientable case. Examples of the implementation of the non-orientable scenarios are given in the case of three-dimensional non-orientable generalized Hénon maps.

Published under license by AIP Publishing. <https://doi.org/10.1063/5.0039870>

In the theory of dynamical systems, the topics related to the construction and study of scenarios of the dynamical chaos onset are ones of the most prioritized and demanded not only for the theory itself, but also for the numerous applications. The pioneering works by Lorenz,<sup>1</sup> Hénon,<sup>2</sup> and Shilnikov<sup>3</sup> laid the foundation for the topics connected with the study of strange homoclinic attractors, i.e., such attractors that contain either equilibria in the case of flows or fixed (periodic) points in the case of maps along with all homoclinic orbits. For three-dimensional maps, the problem of studying discrete homoclinic attractors and scenarios for their occurrence was stated in Ref. 4. This research was continued in a series of papers, but the case of non-orientable maps was not studied in detail. In the present paper, we analyze scenarios of the appearance of discrete homoclinic attractors of non-orientable three-dimensional maps from two different but complementary positions: we construct abstract phenomenological scenarios for the appearance of such attractors and also find examples of their implementation in one-parameter families of three-dimensional non-orientable Hénon-like maps. We distinguish four types of

such non-orientable discrete attractors: Lorenz-like and figure-8 (which contain saddles) as well as spiral figure-8 and Shilnikov attractors (which contain saddle-foci with the one-dimensional and two-dimensional unstable manifolds, respectively). We show features of phenomenological scenarios and compare them with the scenarios for similar attractors in the orientable case. We also discuss some new methods (saddle charts, generalized Lya-punov diagrams) that essentially simplify the process of finding of strange homoclinic attractors.

## I. INTRODUCTION

In the theory of dynamical chaos, phenomenological (purely theoretical, not connected with concrete models) scenarios of its occurrence play an important role since they allow one to explain mechanisms of the formation of chaotic dynamics in experiments from quite simple positions. Besides, such scenarios can open new directions of study, which include, as an integral part, questions of

their realizations in concrete models. Many of these scenarios that underlie the theory of dynamical chaos have been well known for a long time. One can point out such famous and classical scenarios of the chaos appearance as the Landau–Hopf scenario as a result of an infinite cascade of adding frequencies,<sup>5,6</sup> the Ruelle–Takens scenario at the destruction of a three-dimensional torus,<sup>7</sup> the Feigenbaum scenario via an infinite cascade of period doubling bifurcations in strongly dissipative systems,<sup>8</sup> the Afraimovich–Shilnikov scenarios through the break-down of two-dimensional tori,<sup>9</sup> etc. Their phenomenology may be quite simple, but arising here, mathematical problems as well as the questions of realization are always extremely complicated.

In the present paper, we also consider the topic of phenomenological scenarios, but our subject is three-dimensional dissipative diffeomorphisms. We study scenarios of the appearance of the so-called discrete homoclinic attractors, and we construct examples of their implementation in one-parameter families of three-dimensional generalized Hénon maps of the form

$$\bar{x} = y, \bar{y} = z, \bar{z} = Bx + G(y, z), \tag{1}$$

where  $B$  is the Jacobian of the map and  $G(y, z)$  is a smooth function of the coordinates  $y$  and  $z$  only [usually,  $G(y, z)$  is a polynomial].

Following Ref. 4, we call a *discrete homoclinic attractor* a strange attractor of a map that contains exactly one saddle fixed point  $O$  whose invariant stable and unstable manifolds intersect and have transversal homoclinic orbits. Thus, the attractor should also contain entirely the unstable invariant manifold  $W^u(O)$  of this point. The last fact is evident since if there is a point of  $W^u(O)$  that does not belong to the attractor, then the fixed point does not belong to the attractor either. Indeed, in this case, arbitrary close to  $O$ , there exist points whose forward iterations leave the attractor.

**Remark 1.** *This situation is well known for the famous Hénon attractor, see, e.g., Ref. 10, where it is shown that a stable 115-periodic orbit exists with a narrow basin of attraction of size  $10^{-51}$  nearly (up to distance  $10^{-22}$ ) the classical values of the parameters  $a = 1.4, b = 0.3$  of Ref. 2. This is such a subtle effect that it is impossible to detect it with standard numerical methods. However, what is valuable is that, in the case of three-dimensional maps, discrete homoclinic attractors can be genuine pseudohyperbolic attractors<sup>11,12</sup>*

where all two-dimensional areas are exponentially expanded, which implies that any orbit of attractor has a positive maximum Lyapunov exponent. These issues are outside the scope of the present paper.

Discrete homoclinic attractors can be of various types. First, one distinguishes attractors by the type of the saddle fixed points. In the three-dimensional case, these are saddle points either of type (2,1) with the two-dimensional stable and one-dimensional unstable manifolds or of type (1,2) with the one-dimensional stable and two-dimensional unstable manifolds. Second, they are divided into saddles when all eigenvalues of the fixed point are real and saddle-foci when there is a pair of complex conjugate eigenvalues. In addition, it is also natural that saddle points differ by the type of orientability of maps in the restriction to their invariant manifolds, and, certainly, they are different for orientable and non-orientable maps. Recall that a diffeomorphism of  $\mathbb{R}^n$  is called *orientable* or *orientation-preserving* if it has positive Jacobian at all points of  $\mathbb{R}^n$ , and, otherwise, when the Jacobian is negative everywhere, it is called *non-orientable* or *orientation-reversing*. In the present paper, we will consider mainly non-orientable case.

The idea of constructing bifurcation scenarios of the appearance of discrete homoclinic attractors was motivated by Shilnikov's work<sup>3</sup> where a phenomenological scenario for the appearance of a spiral Shilnikov attractor in three-dimensional flows was described. The Shilnikov attractor appears as a result of a simple chain of bifurcations that occur when a parameter varies. We display this scenario in Fig. 1:

- (i) at the beginning, the attractor is a stable equilibrium  $O_\mu$ , Fig. 1(a), then an Andronov–Hopf bifurcation occurs, and  $O_\mu$  becomes a saddle-focus of type (1,2) (with eigenvalues  $\lambda, \gamma \pm i\omega$ , where  $\lambda < 0, \gamma > 0, \omega \neq 0$ ) and a new attractor appears, which is a stable limit cycle  $L_\mu$ , Fig. 1(b);
- (ii) a “differentiable bifurcation” of  $L_\mu$  takes place when the multipliers become a complex conjugate; in this case,  $W^u(O)$  begins to wind of  $L_\mu$ , and the so-called “Shilnikov funnel” is formed into which all the orbits from an absorbing region are drawn, Fig. 1(c); and
- (iii) a spiral Shilnikov attractor emerges when a homoclinic orbit appears for  $O_\mu$ , Fig. 1(d).

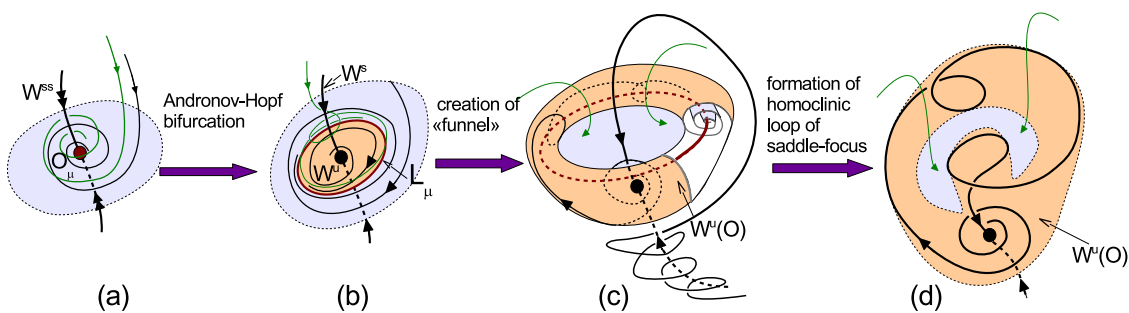


**FIG. 1.** Main steps of the classical Shilnikov scenario for flows, which leads to the appearance of a spiral attractor containing a saddle-focus equilibrium with the two-dimensional unstable manifold: (a)⇒(b) a stable fixed point  $O_\mu$  becomes saddle-focus and a stable limit cycle  $L_\mu$  appears after an Andronov–Hopf bifurcation, (b)⇒(c) a Shilnikov funnel near  $L_\mu$  is formed, and (c)⇒(d) a Shilnikov attractor is created.

As we see, this scenario is distinguished first of all by the simplicity and, of course, it is universal since it is observed in one-parameter families with simple and natural bifurcations. Moreover, as we know, this Shilnikov scenario occurs in a wide variety of models, see, e.g., Ref. 13.

In the case of flows with symmetry, it is natural to expect that the number of universal (in one-parameter families) scenarios, which lead to homoclinic attractors, increases since scenarios associated with the formation of double homoclinic loops of equilibria with one-dimensional unstable manifolds are added up. Perhaps, the most famous such scenario is the scenario of the Lorenz attractor. In the case of the Lorenz model, such a scenario (for  $b = 8/3, \sigma = 28$  and a governing parameter  $r$ ) was described in Refs. 14–16.

Yet, in Ref. 3, it was outlined that analogous scenarios can be naturally expected in the case of maps and that they could be presented as universal scenarios for discrete homoclinic attractors (or for *Poincaré attractors* in the terminology of Ref. 3). However, for a long time, such scenarios were not studied, apparently, for reasons that there were no known examples of discrete analogs of the spiral and Lorenz attractors.

The discrete Lorenz-like attractors were discovered in Ref. 17 for three-dimensional Hénon maps of the form (1) with  $G(y, z) = M_1 + M_2 y - z^2$ . Therefore, natural questions have arisen connected with the study how these attractors appear in one-parameter families starting with simple dynamics. In this connection, in Ref. 4, scenarios for certain types of discrete homoclinic attractors (including Lorenz-like ones) of three-dimensional orientable maps were proposed, as well as some examples of their implementation were demonstrated for the case of maps of the form (1). This topic was continued and expanded in Refs. 12 and 18–20, and, moreover, various discrete homoclinic attractors were also found in applications, in particular, in some models of rigid body dynamics.<sup>21–24</sup>

In the present paper, we study bifurcation scenarios of the appearance of discrete homoclinic attractors in one-parameter families of three-dimensional *non-orientable* maps. We assume that all these scenarios start with the simplest attractor, an asymptotically stable fixed point with eigenvalues  $\lambda_1, \lambda_2, \lambda_3$ , where  $|\lambda_i| < 1$ . We also assume that, for some parameter value, this point loses stability under a soft (supercritical) non-degenerate bifurcation. This bifurcation can be only either a supercritical *period doubling* bifurcation, when exactly one eigenvalue,  $\lambda_1$ , goes through  $\lambda_1 = -1$ , or a supercritical discrete *Andronov-Hopf* bifurcation, when a pair of eigenvalues,  $\lambda_1, \lambda_2$  goes through the unit circle in points  $\lambda_1, \lambda_2 = e^{\pm i\psi}$ , where  $\psi \neq \{0, \pi, 2\pi/3, \pi/2\}$ .

**Remark 2.** Note that there is another possibility when some eigenvalue goes through the value  $\lambda = 1$ , which, in the general case, corresponds to a discrete saddle-node bifurcation after which the fixed point disappears (thus, this bifurcation is rigid, not soft or supercritical). After such bifurcation, the attractor is lost and we should start again. However, a bifurcation through  $\lambda = 1$  can also be soft, and this is a degenerate (codimension 2) pitchfork bifurcation. By these reasons, we do not consider the case of transitions through  $\lambda = 1$ . Nevertheless, it is worth mentioning that pitchfork bifurcations can be generic for maps with global symmetries. Note also that, in the orientable case, scenarios with  $\lambda = 1$  for maps with global symmetries were partially observed in Ref. 20.

We show that four different types of bifurcation scenarios for the appearance of discrete homoclinic attractors are possible in general one-parameter families of three-dimensional non-orientable maps. Specifically, these scenarios result in non-orientable discrete Lorenz-like, figure-8, spiral figure-8, and Shilnikov attractors.

In the scenarios of the first three attractors, the stable fixed point loses stability under a period doubling bifurcation, after which the fixed point becomes saddle of type (2,1), with eigenvalues  $\lambda_1 < -1$  and  $|\lambda_2| < 1, |\lambda_3| < 1$ , and a stable 2-periodic orbit emerges. When the 2-periodic orbit loses stability, a new homoclinic attractor can appear when the two-dimensional stable and one-dimensional unstable manifolds of the fixed point start intersecting. Since the unstable eigenvalue  $\lambda_1$  is negative, double homoclinic intersections are created (as in flows with symmetries). Moreover, the shape of the double homoclinic structures and, hence, the shape of the corresponding homoclinic attractors, depend essentially on the two stable eigenvalues  $\lambda_2$  and  $\lambda_3$  of the fixed point. Thus, we can classify the various cases of scenarios (with  $\lambda_1 < -1$ ) as follows:

- $0 < \lambda_3 < \lambda_2 < 1$  in the Lorenz-like case;
- $-1 < \lambda_2 < \lambda_3 < 0$  in the figure-8 case; and
- $\lambda_2, \lambda_3 = \lambda e^{\pm i\psi}$  and  $0 < \lambda < 1$  in the spiral figure-8 case.

In these three cases, the desired homoclinic attractors are associated with the formation of double homoclinic configurations of saddle fixed points of type (2,1) such as a “homoclinic butterfly,” a “homoclinic figure-8,” and a “spiral figure-8,” respectively. We consider the scenarios for these attractors in Secs. II and III A. It is worth noting that we especially focus on the cases where the unstable eigenvalue of the fixed point  $O$  is negative. Then, the one-dimensional unstable manifold of  $O$  consists of two connected components, separatrices  $\Gamma_1$  and  $\Gamma_2$ , which are symmetric to each other due to the negativity of the unstable eigenvalue. Accordingly, only double homoclinic configurations can arise, i.e., if  $\Gamma_1$  intersects  $W^s(O)$ ,  $\Gamma_2$  intersect it as well and vice versa.

The discrete Shilnikov attractors are considered in Sec. III B, and their appearance is connected with the formation of homoclinic configurations of saddle-focus fixed points of type (1,2). Within the framework of the corresponding scenario, such a point is created after a supercritical discrete Andronov-Hopf bifurcation of a stable fixed point. In the non-orientable case, a saddle-focus (1,2) has eigenvalues  $\lambda, \gamma e^{\pm i\psi}$ , where  $-1 < \lambda < 0$  and  $\gamma > 1, \psi \neq \{0, \pi\}$ . Thus, we have local symmetry between the stable manifolds of the fixed point. For orientable maps, when  $0 < \lambda < 1$ , there is no such symmetry in general (it can appear only in special classes of maps with global symmetries), and, therefore, orientable and non-orientable discrete Shilnikov attractors have different structures (see Sec. III C). Thus, an orientable Shilnikov attractor is one-sided since the fixed point  $O$  lies on the boundary of the attractor and  $W^u(O)$  accumulates to  $W_{loc}^u(O)$  from exactly one side. In contrast, a non-orientable Shilnikov attractor is two-sided: the point  $O$  lies inside the attractor and  $W^u(O)$  accumulates to  $W_{loc}^u(O)$  from both sides (compare Figs. 8 and 10).

The paper is organized as follows. In Sec. II, we describe scenarios of the appearance of non-orientable discrete Lorenz-like and figure-8 attractors and provide also a comparative analysis with the orientable case. In Sec. III, we study scenarios of the appearance of two types of non-orientable spiral (spiral figure-8 and

Shilnikov) attractors. In addition, in Sec. III C, we show the differences between orientable and non-orientable Shilnikov attractors. In Sec. IV, we recall the methods (based on saddle charts and generalized Lyapunov diagrams) for numerical finding regions with the corresponding homoclinic attractors. In Sec. V, we provide numerical implementation of the scenarios described in Secs. II and III in one-parameter families of three-dimensional non-orientable generalized Hénon maps of the form (1) with  $-1 < B < 0$ . Finally, in Sec. VI, we give concluding remarks and discuss open problems on the related topics.

## II. NON-ORIENTABLE DISCRETE LORENZ-LIKE AND FIGURE-8 ATTRACTORS

In this section, we give a description of scenarios for the appearance of non-orientable discrete Lorenz and figure-8 homoclinic attractors, which contain saddle fixed points with homoclinic orbits, in Secs. II A and II B. We also give a comparative analysis of these scenarios with the similar scenarios of three-dimensional orientable maps in Sec. II C.

### A. Scenarios for non-orientable discrete Lorenz-like attractors

A scenario for the appearance of non-orientable discrete Lorenz-like attractors is outlined in Fig. 2. Let us consider a non-orientable map  $T_\mu$ . We start with the values of the parameter  $\mu$  where  $T_\mu$  has a stable fixed point  $O_\mu$ , Fig. 2(a). We assume that when  $\mu$  varies, as a result of a *supercritical period doubling bifurcation*,  $O_\mu$  loses stability and becomes a saddle of type (2,1) with the unstable eigenvalue  $\lambda_1 < -1$  and a stable 2-periodic orbit  $(p_1, p_2)$  appears, Fig. 2(b).

When  $\mu$  changes further, various bifurcations can occur, and we emphasize the most important of them:

- bifurcations after which the orbit  $(p_1, p_2)$  and all attracting invariant sets generated from it lose their stability and
- global bifurcations of the creation of homoclinic orbits to  $O_\mu$  when the unstable separatrices  $\Gamma_1$  and  $\Gamma_2$  of  $O_\mu$  start intersecting  $W^s(O_\mu)$ .

Recall that, when  $W^u(O_\mu)$  is one-dimensional,  $\Gamma_1$  and  $\Gamma_2$  are two connected components of  $W^u(O_\mu) \setminus O_\mu$ . Since the unstable eigenvalue  $\lambda_1$  of  $O_\mu$  is negative, it is true that  $T_\mu(\Gamma_1(\mu)) = \Gamma_2(\mu)$  and  $T_\mu(\Gamma_2(\mu)) = \Gamma_1(\mu)$ . Therefore, if  $\Gamma_1$  intersects  $W^s(O_\mu)$ , then  $\Gamma_2$  also intersects it and vice versa. Thus, homoclinic intersections of the saddle  $O_\mu$  appear in pairs as double homoclinic orbits. In the case under consideration, this double homoclinic configuration is associated with the saddle fixed point  $O_\mu$  whose eigenvalues  $\lambda_1, \lambda_2, \lambda_3$  satisfy the following condition, which can be considered the characteristic condition for the scenario:

$$\lambda_1 < -1, 0 < \lambda_3 < \lambda_2 < 1, -1 < \lambda_1 \lambda_2 \lambda_3 < 0, \quad (2)$$

$$\sigma = |\lambda_1| |\lambda_2| > 1,$$

where  $\sigma$  is the so-called *saddle value* of  $O_\mu$ . Recall that the saddle value of a saddle fixed point is defined generally as the absolute value of the product of the two nearest to the unit circle eigenvalues such that one eigenvalue is stable (less than 1 in modulus) and the other is unstable (greater than 1 in modulus).

When condition (2) holds and the separatrices  $\Gamma_1$  and  $\Gamma_2$  intersect  $W^s(O_\mu)$ , their configuration, see Figs. 2(c) and 2(d), is similar to the famous homoclinic butterfly in the Lorenz model. In particular, when  $W^u(O_\mu)$  starts intersecting  $W^s(O_\mu)$ , a pair of primary homoclinic orbits with points  $(h_1, h_2, \dots)$  and  $(h^1, h^2, \dots)$  in  $W_{loc}^s$  is created, as shown schematically in Fig. 2(c). These orbits contain points belonging alternately to  $\Gamma_1$  and  $\Gamma_2$ . Thus,  $h_1 \in \Gamma_1, h_2 = T_\mu(h_1) \in \Gamma_2, h_3 = T_\mu(h_2) \in \Gamma_1, \dots$ , as well as  $h^1 \in \Gamma_1, h^2 = T_\mu(h^1) \in \Gamma_2, h^3 = T_\mu(h^2) \in \Gamma_1, \dots$ . Note also that the bifurcation of the creation of a homoclinic butterfly is accompanied by infinitely many periodic orbits and closed invariant curves. In particular, a 2-periodic closed invariant curve  $(C_1, C_2)$  is formed. This curve is of saddle type when  $\sigma > 1$ . In the case  $\sigma < 1$ , the curve  $(C_1, C_2)$  is stable, which means that it is an attractor, and the further development of chaos can proceed through the destruction of this curve and the appearance of a torus-chaos, for example, but not a homoclinic attractor at all. Therefore, the condition  $\sigma > 1$  is principally important.

It is worth noting that even when the homoclinic butterfly is formed, the orbit  $(p_1, p_2)$  can remain stable and it may be either a

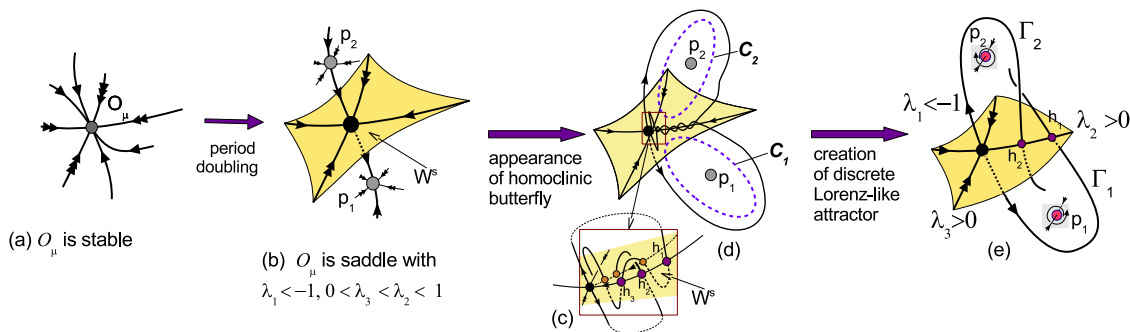


**FIG. 2.** A bifurcation scenario for a discrete Lorenz-like attractor in non-orientable three-dimensional maps. The path is as follows. (a)⇒(b): A period doubling bifurcation of stable fixed point  $O_\mu$  takes place, after which  $O_\mu$  becomes saddle of type (2,1) and a stable 2-periodic orbit  $(p_1, p_2)$  appears; (b)⇒(c) and (d): a homoclinic butterfly is formed, in (c) primary homoclinic points in  $W_{loc}^s(O_\mu)$  are displayed; (d)⇒(e): a discrete Lorenz-like attractor emerges.

unique attractor of the map or can coexist with a homoclinic attractor. We are interested in the case when the orbit  $(p_1, p_2)$  and all stable sets generated from it lose stability. The loss of stability depends on the model under consideration. However, one can specify the two simplest options (see also Ref. 12):

- (i) the stable orbit  $(p_1, p_2)$  undergoes a subcritical Andronov–Hopf bifurcation, merges with the curve  $(C_1, C_2)$ , and becomes a 2-periodic saddle-focus of type (1,2) and
- (ii) the stable orbit  $(p_1, p_2)$  undergoes a supercritical Andronov–Hopf bifurcation after which it becomes a 2-periodic saddle-focus of type (1,2) and a 2-periodic stable closed invariant curve  $(S_1, S_2)$  shows up and then this curve merges with the 2-periodic saddle curve  $(C_1, C_2)$  and both disappear (via a Chenciner bifurcation<sup>25</sup>).

Note that the flow analogs of options (i) and (ii) are realized, respectively, in the Lorenz model<sup>14</sup> and the Shimizu–Morioka model.<sup>26</sup> In Refs. 12 and 24, it was shown that these options can also be observed in the case of three-dimensional maps with orientable discrete Lorenz-like attractors.

We can summarize the main stages of the scenario (in a one-parameter family  $T_\mu$  when  $\mu$  changes) as follows (see also Fig. 2):

- (a) the attractor is a non-orientable stable fixed point  $O_\mu$ ;
- (b) after a period doubling bifurcation of  $O_\mu$ : the attractor is a 2-periodic orbit  $(p_1, p_2)$ ; the point  $O_\mu$  becomes a non-orientable saddle of type (2,1) with  $\lambda_1 < -1$ ;
- (c) and (d) the creation of a homoclinic butterfly of the saddle point  $O_\mu$  whose eigenvalues satisfy condition (2), takes place, the attractor can be still the orbit  $(p_1, p_2)$ ; and
- (e) the formation of a discrete Lorenz-like attractor occurs after  $(p_1, p_2)$  and all stable invariant orbits generated from it lose stability.

### B. Scenarios for non-orientable discrete figure-8 attractors

A scenario for a non-orientable discrete figure-8 attractor is presented in Fig. 3. The beginning of this scenario is the same as in the Lorenz-like attractor case. First, the map  $T_\mu$  has an asymptotically stable fixed point  $O_\mu$ , which undergoes a period doubling bifurcation, and  $O_\mu$  becomes a saddle of type (2,1) and a stable 2-periodic orbit  $(p_1, p_2)$  emerges; see Figs. 3(a) and 3(b). The principle difference is that the eigenvalues of the point  $O_\mu$  satisfy the following conditions when homoclinic orbits of  $O_\mu$  appear:

$$\lambda_1 < -1 < \lambda_3 < \lambda_2 < 0 \text{ and } \sigma = |\lambda_1||\lambda_3| > 1, \quad (3)$$

which is the characteristic condition for the figure-8 scenario.

Then, the double homoclinic configuration, appearing when the invariant manifolds of the point  $O_\mu$  start intersecting, resembles a homoclinic figure-8 of a saddle equilibrium for a flow. Therefore, such attractor was called a *discrete figure-8 attractor* in Ref. 4. In Figs. 3(c) and 3(d), the moment of creation of this double homoclinic orbit is shown when a pair of primary homoclinic orbits with points  $(h_1, h_2, \dots)$  and  $(h^1, h^2, \dots)$  in  $W_{loc}^s$  are formed, as shown schematically in Fig. 3(c). These orbits contain points that belong to  $\Gamma_1$  and  $\Gamma_2$  alternately. Thus,  $h_1 \in \Gamma_1, h_2 = T_\mu(h_1) \in \Gamma_2, h_3 = T_\mu(h_2) \in \Gamma_1, \dots$ , as well as  $h^1 \in \Gamma_1, h^2 = T_\mu(h^1) \in \Gamma_2, h^3 = T_\mu(h^2) \in \Gamma_1, \dots$ ; see Fig. 3(c).

Note also that as in the previous case of a discrete homoclinic butterfly, a 2-periodic saddle closed invariant curve  $(C_1, C_2)$  appears when a discrete figure-8 with  $\sigma > 1$  is formed, and, besides, options (i) and (ii) can be feasible for a non-orientable discrete figure-8 attractor.

We summarize the main stages of the scenario for a non-orientable discrete figure-8 attractor (in a family  $T_\mu$  when  $\mu$  varies) as follows (see also Fig. 3):

- (a) the attractor is a non-orientable stable fixed point  $O_\mu$ ;
- (b) the attractor is a 2-periodic orbit  $(p_1, p_2)$ ; after a period doubling bifurcation, the point  $O_\mu$  becomes a non-orientable saddle of type (2,1) with  $\lambda_1 < -1$ ;

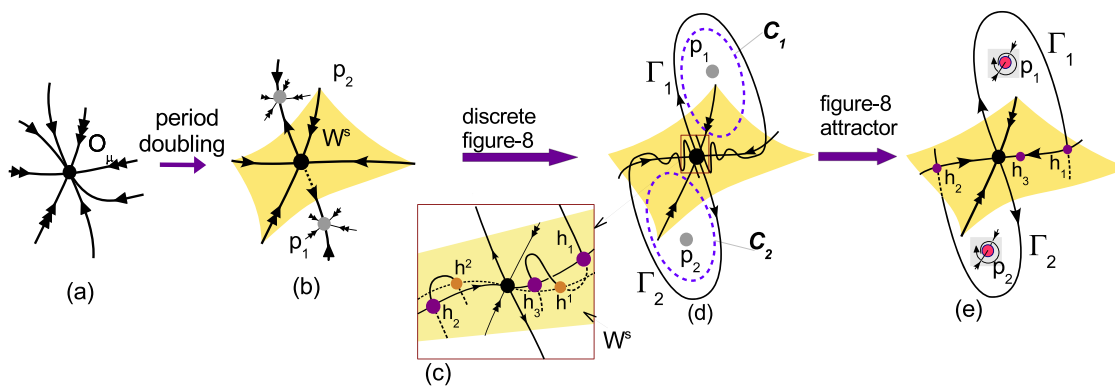


**FIG. 3.** A bifurcation scenario for a non-orientable discrete figure-8 attractor in three-dimensional maps: (a)⇒(b) after a period doubling bifurcation, the stable fixed point  $O_\mu$  becomes saddle and a 2-periodic stable orbit  $(p_1, p_2)$  appears; (b)⇒(c) and (d) a homoclinic figure-8 is created, in (c) the disposition of primary homoclinic points is shown in  $W_{loc}^s(O_\mu)$ ; and (d)⇒(e) a discrete homoclinic figure-8 attractor appears.

- (c) and (d) the creation of a homoclinic figure-8 of the saddle point  $O_\mu$  whose eigenvalues satisfy condition (3) takes place, and the attractor is the orbit  $(p_1, p_2)$ ; and
- (e) the formation of a discrete figure-8 attractor occurs after  $(p_1, p_2)$  and all stable invariant sets generated from it lose stability.

**C. Comparative analysis with the orientable case**

In this section, we can point out similarities and differences in the scenarios for discrete Lorenz-like and figure-8 attractors of orientable and non-orientable maps. In both orientable and non-orientable cases, the scenarios start similarly with a period doubling bifurcation of a stable fixed point, which loses stability and turns into a saddle (2,1), and an attracting 2-periodic orbit appears. After that, the orientable and non-orientable scenarios differ in specific details.

Scenarios of orientable discrete Lorenz-like attractors in the case of one-parameter families of three-dimensional maps were proposed in Ref. 4 and studied in detail in Refs. 12, 19, and 20. We outline the “homoclinic” stages of the scenarios for the orientable and non-orientable cases in Figs. 4(b) and 4(d), respectively. The first thing to notice is that the fixed points have different topological

types. In the orientable case, the eigenvalues of the point  $O_\mu$  satisfy the condition

$$\lambda_1 < -1 < \lambda_3 < 0 < \lambda_2 < 1, \quad 0 < \lambda_1 \lambda_2 \lambda_3 < 1, \quad (4)$$

$$|\lambda_2| > |\lambda_3|, \sigma = |\lambda_1| |\lambda_2| > 1,$$

while, in the non-orientable case, condition (2) is fulfilled.

Let us define a two-dimensional map  $\tilde{T}_s$  as restriction of  $T_\mu$  in a two-dimensional disk  $W_{loc}^s$ , i.e.,  $\tilde{T}_s = T_\mu|_{W_{loc}^s}$ . This map is non-orientable if map  $T_\mu$  is orientable and is orientable if map  $T_\mu$  is non-orientable. The fixed point  $\tilde{O}$  of  $\tilde{T}_s$  has eigenvalues  $0 < \lambda_2 < 1, -1 < \lambda_3 < 0$  where  $|\lambda_3| < |\lambda_2|$ , in the first case, and  $0 < \lambda_3 < \lambda_2 < 1$ , in the second case. In both cases, in  $W_{loc}^s$ , there is the so-called strong stable one-dimensional invariant manifold  $W^{ss}$ , which goes to  $\tilde{O}$  along the direction corresponding to the eigenvalue  $\lambda_3$  and divides  $W_{loc}^s$  into two parts. In the cases under consideration, all homoclinic points to  $\tilde{O}$  in  $W_{loc}^s$  belong to the same part, but their location is different [compare Figs. 4(b) and 4(d)].

Notice that in the general case, a homoclinic attractor can be presented as the closure of the unstable manifold of the fixed point  $O_\mu$  (see Remark 1). Since the unstable separatrices  $\Gamma_1$  and  $\Gamma_2$  of the saddle  $O_\mu$  accumulate to themselves (forming a one-dimensional

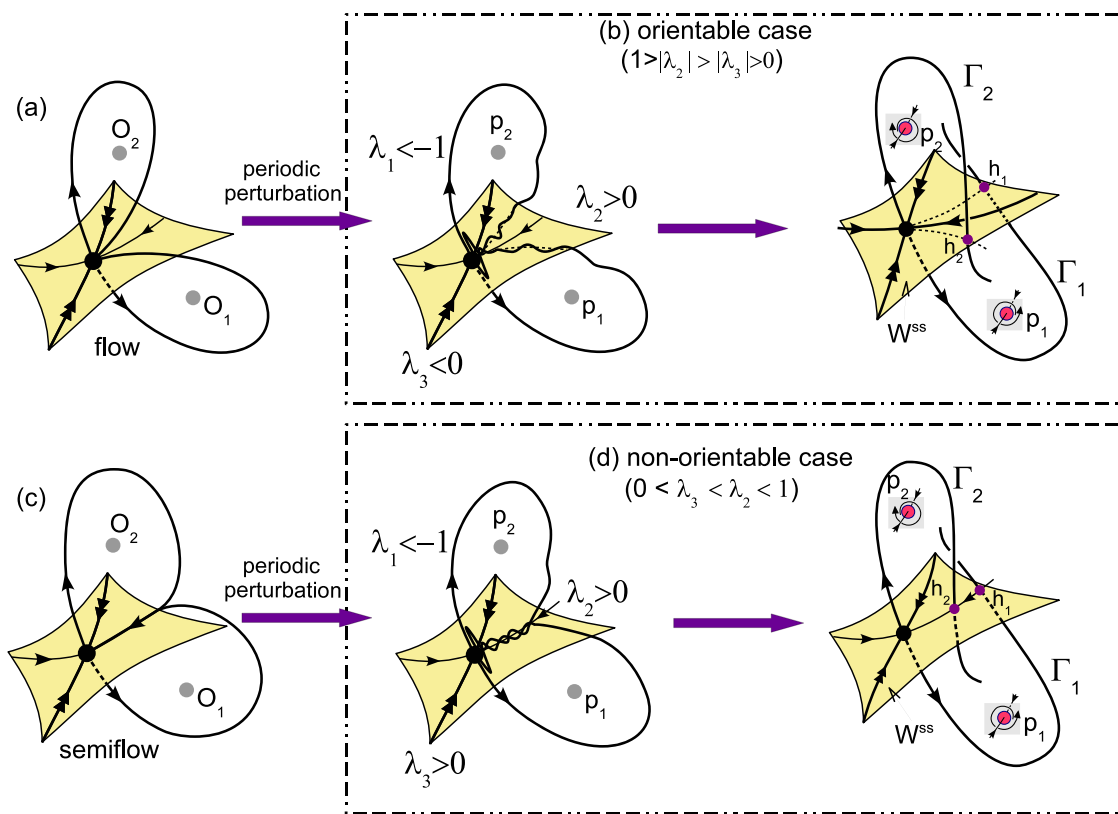


**FIG. 4.** Toward a comparison of scenarios for discrete Lorenz-like attractors in (a) and (b) the orientable case and in (c) and (d) the non-orientable case. In the orientable case (a), a discrete homoclinic configuration can be obtained as a result of an arbitrary small smooth periodic perturbation of a three-dimensional flow with a homoclinic butterfly, while, in the non-orientable case (c), this can be obtained only by a periodic perturbation of a semiflow (when the unstable separatrices partially coincide).

indecomposable continuum), their homoclinic points in  $W_{loc}^s(O_\mu)$  lie near the primary homoclinic points  $h_1, h_2, \dots$  and  $h^1, h^2, \dots$  [see Figs. 2(c) and 2(e)].

Let us consider the points  $h_1, h_2, \dots$ , where  $h_1$  and  $h_2$  are the first intersection points of the disk  $W_{loc}^s(O_\mu)$  and the separatrices  $\Gamma_1$  and  $\Gamma_2$ , respectively. For  $T^2(\mu)$ , the separatrices  $\Gamma_1$  and  $\Gamma_2$  are invariant, and, thus, the points  $h_1, h_3, \dots, h_{2i+1}, \dots$  and  $h_2, h_4, \dots, h_{2i}, \dots$  are homoclinic points for  $T^2(\mu)$ , which belong to  $\Gamma_1$  and  $\Gamma_2$ , respectively. When  $T_\mu$  is orientable and  $\tilde{T}_s$  is non-orientable, these homoclinic points reside in different smooth invariant curves, which are tangent at  $O_\mu$  [Fig. 5(a)]. This is consistent with the fact that a discrete homoclinic butterfly for  $T_\mu^2$  can be represented in the Poincaré map for a small smooth periodic perturbation of a three-dimensional flow with a homoclinic butterfly as in Fig. 4(a).

If  $T_\mu$  is non-orientable, since eigenvalues  $\lambda_2$  and  $\lambda_3$  of the fixed point  $\tilde{O}$  of the orientable map  $\tilde{T}_s$  are positive, all the homoclinic points  $h_1, h_2, \dots$  lie in the same smooth invariant curve, which tends to  $\tilde{O}$  [Fig. 5(b)]. Accordingly, for  $T^2(\mu)$ , the homoclinic points  $\{h_1, h_3, \dots, h_{2i+1}, \dots\} \in \Gamma_1$  and  $\{h_2, h_4, \dots, h_{2i}, \dots\} \in \Gamma_2$  also lie in the same curve. Therefore, in the corresponding imagined non-perturbed flow system, the separatrices  $\Gamma_1$  and  $\Gamma_2$  should go to the equilibrium along the same orbit. This is impossible for a flow, but a semiflow can possess such a configuration, as in Fig. 4(c).

The fact that an orientable discrete Lorenz-like attractor for  $T^2(\mu)$  can be obtained as a result of a small periodic perturbation of

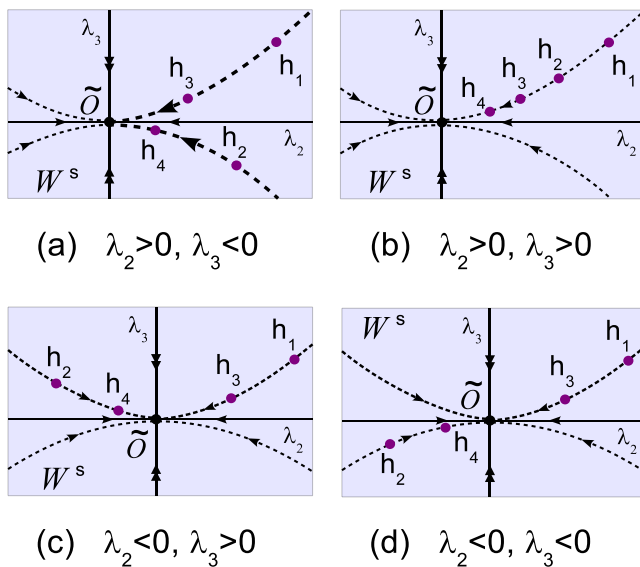


**FIG. 5.** Orbit behavior of  $\tilde{T}_s$  near a stable fixed point  $\tilde{O}$  with real eigenvalues  $\lambda_2$  and  $\lambda_3$ , where  $0 < |\lambda_3| < |\lambda_2| < 1$  and (a)  $\lambda_2 > 0, \lambda_3 < 0$ ; (b)  $\lambda_2 > 0, \lambda_3 > 0$ ; (c)  $\lambda_2 < 0, \lambda_3 > 0$ ; and (d)  $\lambda_2 < 0, \lambda_3 < 0$ . We consider various possible cases, and, for the sake of simplicity, we assume that the map  $\tilde{T}_s$  is linear:  $\bar{x} = \lambda_2 x, \bar{y} = \lambda_3 y$ . A neighborhood of  $\tilde{O}$  is foliated into invariant curves  $y = C|x|^\alpha$ , where  $\alpha = \frac{\ln|\lambda_3|}{\ln|\lambda_2|}$  and  $C$  runs all values from  $-\infty$  to  $+\infty$ . The foliation contains also the leaf  $x = 0$ , which corresponds to the strong stable manifold  $W^{ss}$ .

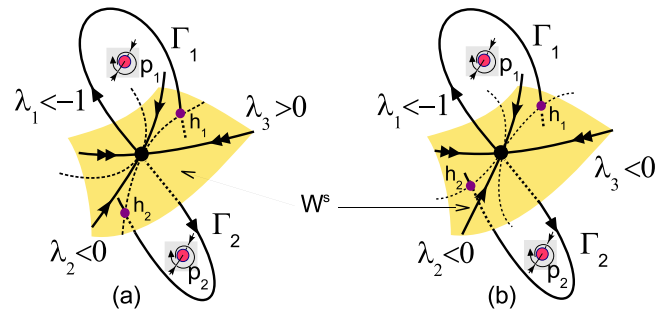


**FIG. 6.** Homoclinic configurations for discrete figure-8 attractors in (a) the orientable case and in (b) the non-orientable case.

a system with the Lorenz attractor (which satisfies conditions of the Afraimovich–Bykov–Shilnikov geometric model<sup>14,27</sup>) was proved in Ref. 28. Besides, it was shown in Ref. 17 that an orientable discrete Lorenz-like attractor can emerge under a local codimension 3 bifurcation of a fixed point with eigenvalues  $(-1, -1, +1)$ . It seems that none of this can be done in the case of a non-orientable discrete Lorenz-like attractor.

As for the orientable and non-orientable discrete homoclinic figure-8 attractors, first of all, they are quite similar. This can be seen from the location of the primary homoclinic points  $h_1, h_2, \dots$ , where  $\{h_1, h_3, \dots, h_{2i+1}, \dots\} \in \Gamma_1$  and  $\{h_2, h_4, \dots, h_{2i}, \dots\} \in \Gamma_2$ , in  $W_{loc}^s(O_\mu)$  [see Figs. 5(c) and 5(d)]. The difference is not so essential, which is also confirmed by the homoclinic schemes for the attractors shown in Fig. 6. Moreover, looking at Figs. 5(c) and 5(d), one can say that for the orientable and non-orientable figure-8 attractors, there are different symmetries in  $W_{loc}^s$  with respect to the strong stable manifold and with respect to  $\tilde{O}$ , respectively.

The other side of the problem is how one can obtain discrete figure-8 attractors by means of periodic perturbations of continuous systems with a figure-8 of a saddle equilibrium. In the case with  $\sigma > 1$ , it is impossible since the figure-8 of the corresponding flow is not an attractor. Accordingly, a possible discrete attractor in the Poincaré map will be located outside of a neighborhood of the figure-8, and, thus, it is not a homoclinic attractor. In the case  $\sigma < 1$ , the attractor may be homoclinic, but we do not consider them since, as said above, scenarios with  $\sigma < 1$  can go in a completely different way.

### III. NON-ORIENTABLE DISCRETE SPIRAL ATTRACTORS

In this section, we observe scenarios of the appearance of non-orientable discrete spiral attractors, which contain saddle-focus fixed points with homoclinic orbits. We consider two types of these attractors: spiral figure-8 attractors with the two-dimensional stable and one-dimensional unstable invariant manifolds in Sec. III A and spiral Shilnikov attractors with the one-dimensional stable and two-dimensional unstable invariant manifolds in Sec. III B. Since orientable maps in the case of saddle fixed points with  $\lambda_1 < -1$  cannot



have discrete spiral figure-8 attractors, we only provide a comparative analysis of orientable and non-orientable discrete Shilnikov attractors in Sec. III C.

**A. Scenarios for non-orientable discrete spiral figure-8 attractors**

A scenario of the appearance of a non-orientable discrete spiral figure-8 attractor is displayed in Fig. 7. This scenario can be considered an intermediate case between the first two scenarios (“Lorenz” and “figure-8”) in the non-orientable case. The point  $O_\mu$  loses stability under a supercritical period doubling bifurcation after which the eigenvalues take values  $\lambda_1 < -1$ ,  $\lambda_2, \lambda_3 = \lambda e^{\pm i\varphi}$ , where  $0 < \lambda < 1$ . Thus, the point  $O_\mu$  becomes a saddle-focus of type (2,1) and a stable 2-periodic orbit  $(p_1, p_2)$  emerges. Accordingly, when  $\mu$  changes further, this 2-periodic orbit loses stability, homoclinic orbits of  $O_\mu$  appear, and a non-orientable discrete homoclinic spiral figure-8 attractor can be formed, which contains the saddle-focus  $O_\mu$  and the one-dimensional unstable manifold [Figs. 7(c) and 7(d)]. One can see that the shape of this attractor depends on the value of  $\varphi$ . When  $\varphi$  is very close to 0, it is similar to a discrete Lorenz-like attractor, compare Figs. 2(e) and 7(c), and when  $\varphi$  is close to  $\pi$ , it resembles a discrete figure-8 attractor [compare Figs. 3(e) and 7(d)].

Note that the scenario for non-orientable discrete spiral figure-8 attractors has no direct analogs in the orientable case. Some asymmetric spiral figure-8 attractors can appear when a fixed point is a saddle-focus of type (2,1) with eigenvalues  $\lambda_1 > 1, \lambda e^{\pm i\varphi}$ , where  $0 < \lambda < 1$ , and both unstable separatrices intersect the stable manifold. If an orientable map admits an appropriate symmetry, for example, as an orientable map of the form (1) with the central symmetry, when  $G(y, z) = -G(-y, -z)$ , then, evidently, symmetric orientable spiral figure-8 attractors can appear. In our case, a non-orientable saddle-focus  $O_\mu$  has eigenvalues  $\lambda_1 < -1, \lambda e^{\pm i\varphi}$ , and, thus, a spiral figure-8 attractor with such point  $O_\mu$  is always symmetric due to negativity of the unstable eigenvalue  $\lambda_1$ .

We also note that in the cases when  $\varphi$  is close to  $\pi/2$  or  $2\pi/3$ , the corresponding spiral figure-8 attractors can take specific forms; see, e.g., Fig. 15 for such an attractor with  $\varphi$  close to  $\pi/2$ .

Unfortunately, we have not observed such attractors for  $\varphi$  close to  $2\pi/3$ , although such an attractor could be quite interesting.

We summarize the scenario for a non-orientable discrete spiral figure-8 attractor in a one-parameter family  $T_\mu$  when  $\mu$  changes as follows (see also Fig. 7):

- (a) the attractor is a non-orientable stable fixed point  $O_\mu$ ;
- (b) the attractor is a 2-periodic orbit  $(p_1, p_2)$  that appears after a period doubling bifurcation; the point  $O_\mu$  becomes a non-orientable saddle-focus of type (2,1); and
- (c) and (d) the orbit  $(p_1, p_2)$  loses stability,  $W^s(O_\mu)$  and  $W^u(O_\mu)$  start intersecting, and a spiral figure-8 attractor appears whose shape depends on the angle  $\varphi$  of the complex eigenvalue of  $O_\mu$ .

**B. Scenarios for non-orientable discrete Shilnikov attractors**

A scenario of the appearance of a non-orientable discrete Shilnikov attractor is illustrated in Fig. 8. This scenario significantly differs from the previous three scenarios (“Lorenz,” “figure-8,” and “spiral figure-8”). In a one-parameter family  $T_\mu$  of three-dimensional maps, it starts with a stable fixed point  $O_\mu$ , Fig. 8(a), however, in this case,  $O_\mu$  loses stability under a discrete *supercritical Andronov-Hopf* bifurcation. After this bifurcation, the point  $O_\mu$  becomes a saddle-focus of type (1,2) with eigenvalues  $\lambda_{1,2} = \gamma e^{\pm i\varphi}, -1 < \lambda_3 < 0$ , where  $\gamma > 1$ , and a stable closed invariant curve  $L_\mu$  emerges [Fig. 8(b)]. Afterward, when  $\mu$  changes, we assume that the curve  $L_\mu$  loses stability.

One of the most interesting and realistic ways of the stability loss is that  $L_\mu$  undergoes a doubling bifurcation. After this bifurcation, the curve  $L_\mu$  becomes a saddle type and two *stable invariant curves*  $\hat{L}_\mu^1$  and  $\hat{L}_\mu^2$  of period 2 [i.e.,  $\hat{L}_\mu^2 = T_\mu(\hat{L}_\mu^1)$  and  $\hat{L}_\mu^1 = T_\mu(\hat{L}_\mu^2)$ ] appear in a neighborhood of  $L_\mu$  (see the transition (b) $\Rightarrow$ (c) in Fig. 8). Each of the curves  $\hat{L}_\mu^1$  and  $\hat{L}_\mu^2$  is invariant with respect to  $T_\mu^2$ , and, hence, when  $\mu$  changes, they can undergo a “differentiable bifurcation” (the curves of a nodal type change to a focal type). As a

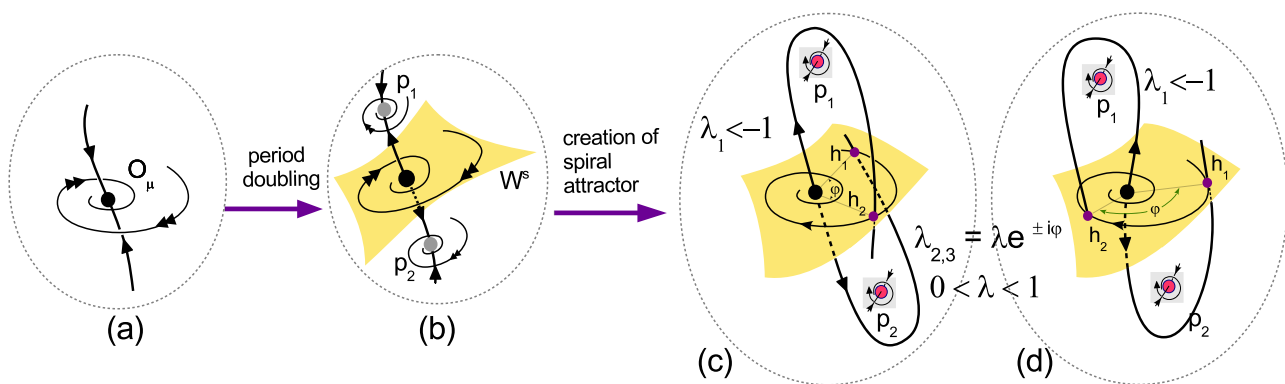


**FIG. 7.** A bifurcation scenario for a spiral figure-8 attractor in non-orientable three-dimensional maps: (a) $\Rightarrow$ (b) stable fixed point  $O_\mu$  becomes saddle-focus after a period doubling bifurcation; (b) $\Rightarrow$ (c) a spiral figure-8 attractor similar to a Lorenz-like attractor appears if  $\varphi$  is close to 0; and (b) $\Rightarrow$ (d) a spiral figure-8 attractor similar to a figure-8 attractor appears if  $\varphi$  is close to  $\pi$ .

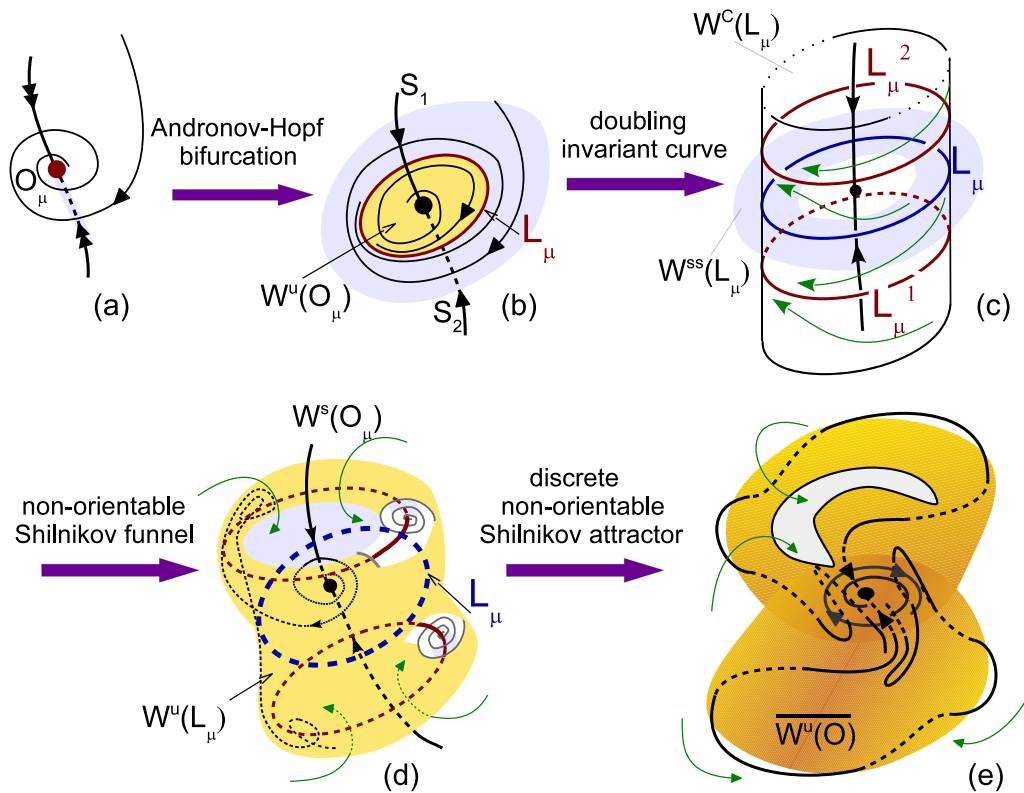


**FIG. 8.** A scenario for a non-orientable discrete Shilnikov attractor: (a)⇒(b) the stable fixed point  $O_\mu$  becomes a saddle-focus and a stable invariant curve  $L_\mu$  emerges after an Andronov–Hopf bifurcation; (b)⇒(c) a doubling bifurcation of  $L_\mu$  occurs and stable invariant curves  $\hat{L}_\mu^1$  and  $\hat{L}_\mu^2$  emerge; (c)⇒(d) a two-sided Shilnikov funnel is created since the curves  $\hat{L}_\mu^1$  and  $\hat{L}_\mu^2$  become a focal type; and (d)⇒(e) homoclinic orbits to  $O_\mu$  appear and a discrete Shilnikov attractor is formed.

result of this reconstruction, the unstable two-dimensional manifold of the saddle  $O_\mu$  begins to wind on both curves  $\hat{L}_\mu^1$  and  $\hat{L}_\mu^2$ , thereby forming a two-sided “Shilnikov funnel,” into which all orbits from the corresponding absorbing region are drawn [see Fig. 8(d)]. Afterward, inside the funnel, all stable invariant sets (including the curves  $\hat{L}_\mu^1$  and  $\hat{L}_\mu^2$ ) lose stability, homoclinic intersections of  $W^s(O_\mu)$  and  $W^u(O_\mu)$  appear, and a non-orientable discrete Shilnikov attractor can be formed [Fig. 8(e)].

In this scenario, we emphasize the step related to the unusual character of a doubling bifurcation of an invariant curve. As is well known, see, e.g., Ref. 29, in the orientable case, such a bifurcation is length-doubling and leads to the appearance of one (stable) invariant curve of double length, which wraps twice around the initial curve, while, in the non-orientable case, a pair of 2-periodic invariant curves of an ordinary length emerges. This difference is closely connected with the topology of the manifolds  $W^u(L)$  and  $W^s(L)$  of a saddle invariant non-resonant curve for diffeomorphisms in  $\mathbb{R}^3$ . Locally, these manifolds are some strips  $W_\delta^s(L)$  and  $W_\delta^u(L)$  of width  $\delta$  that intersect transversally along  $L$ . Evidently, for diffeomorphisms of  $\mathbb{R}^3$ ,  $W_\delta^s(L)$  and  $W_\delta^u(L)$  are both either cylinders or Möbius bands [see Figs. 9(a) and 9(b)]. We illustrate this simple topological fact in Fig. 9(c), where the curve  $L$  is shown inside a

cub  $Q : -1 \leq (x, y, z) \leq 1$  whose faces  $x = 1$  and  $x = -1$  of  $Q$  are supposed to be identified. Let  $W^u(L)$  be a cylinder, in Fig. 9(c), this is the rectangle  $AA'B'B$  with the identified edges  $AB$  and  $A'B'$ . Then,  $W^u(L)$  divides the cube into two connected components,  $0 < y < 1$  and  $-1 < y < 0$ . If  $W^s(L)$  is a Möbius band (a twisted band  $CC'D'D$  with the identified edges  $CD$  and  $C'D'$ ), it also should have intersection points with  $W^u(L)$  (the arc  $\bar{p}, \bar{q}$ ) apart from  $L$ , which is impossible.

When such a diffeomorphism  $T$  of  $\mathbb{R}^3$  is non-orientable, both the strips  $W_\delta^s(L)$  and  $W_\delta^u(L)$  are cylinders. Indeed, one of the two-dimensional maps  $T|_{W_\delta^s}$  and  $T|_{W_\delta^u}$  is orientable (then the other map is non-orientable), which means that the corresponding manifold is orientable; i.e., it is a cylinder. Thus, the other manifold is also a cylinder. If  $L$  undergoes a doubling bifurcation, as usually it occurs along the central manifold  $W^c(L)$ , as shown in Fig. 8(c). Since  $W^c(L)$  is a cylinder, this bifurcation leads to the appearance of 2-periodic invariant curves, which are located on both hands of  $L$  (above and below) in  $W^c(L)$  and have approximately the same length as  $L$ . Note that apparently, the first example of such a bifurcation was considered in Ref. 30 in the case a quasiperiodically driven Hénon map, which is non-orientable ( $J = -0.4$ ) and has a closed invariant curve whose rotation number is the golden mean  $(\sqrt{5} - 1)/2$ .

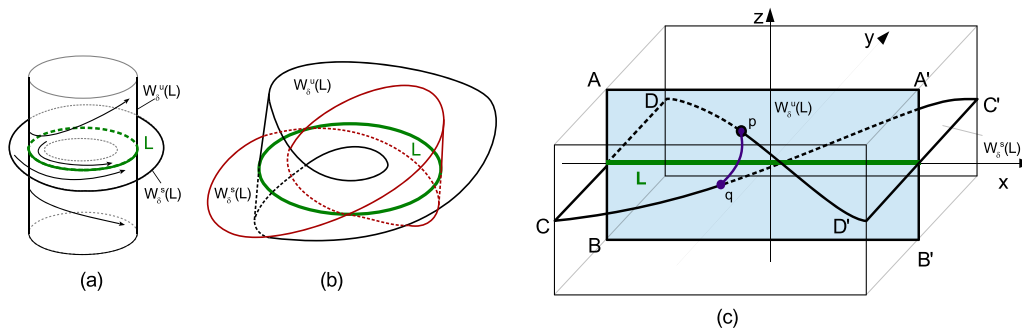


**FIG. 9.** Local stable and unstable invariant manifolds  $W_s^s(L)$  and  $W_s^u(L)$  of a saddle non-resonant curve  $L$  in  $\mathbb{R}^3$  can be either (a) both cylinders or (b) both Möbius bands, but (c) the case when one of them is a cylinder and the other is a Möbius band is impossible.

We summarize the scenario for a non-orientable Shilnikov attractor in a one-parameter family  $T_\mu$  when  $\mu$  changes as follows (see also Fig. 8):

- (a) the attractor is a stable fixed point  $O_\mu$ ;
- (b) the attractor is the invariant curve  $L_\mu$ , which emerges after an Andronov–Hopf bifurcation of  $O_\mu$ ; the point  $O_\mu$  becomes a non-orientable saddle-focus of type (1,2);
- (c) the attractor is the invariant curves  $L_\mu^1$  and  $L_\mu^2$ , which emerge after a doubling bifurcation of  $L_\mu$ ; the curve  $L_\mu$  becomes a saddle type;
- (d) the creation of a two-sided Shilnikov funnel with stable sets occurs; and
- (e) the formation of a non-orientable Shilnikov attractor occurs after all stable invariant sets (including  $\hat{L}_\mu^1$  and  $\hat{L}_\mu^2$ ) lose stability and homoclinic intersections of  $W^s(O_\mu)$  and  $W^u(O_\mu)$  appear.

**C. Comparative analysis with the orientable case**

The main stages of the appearance of Shilnikov attractors differ in details for the non-orientable and orientable cases, compare Figs. 8 and 10, where a scenario for an orientable discrete Shilnikov attractor is illustrated. As in the non-orientable case, the orientable scenario starts with a stable fixed point  $O_\mu$ , Fig. 10(a),

which loses stability under a supercritical Andronov–Hopf bifurcation:  $O_\mu$  becomes a saddle-focus of type (1,2) and there appears a stable invariant curve  $L_\mu$ , which is the new attractor [Fig. 10(b)]. Since the stable eigenvalue  $\lambda_3$  is positive, the stable separatrices  $S_1$  and  $S_2$  are invariant, i.e.,  $T_\mu(S_1) = S_1$ ,  $T_\mu(S_2) = S_2$ , and their behavior is independent.

As one can see in Figs. 8 and 10, the main difference in the orientable and non-orientable scenarios is connected with the formation of the Shilnikov funnel. In the orientable case, the funnel appears due to a “differentiable bifurcation” when the curve  $L_\mu$  changes the type from nodal to focal,<sup>4,19</sup> Fig. 10(c), and all orbits from an absorbing domain, except those in the stable separatrix  $S_2$ , go inside the funnel. Thus, the orientable funnel is one-sided (as a “sac”). We note that in the orientable case, both manifolds  $W^s(L_\mu)$  and  $W^u(L_\mu)$  are Möbius bands [see Fig. 9(b)]. A homoclinic attractor can be created when  $W^u(O_\mu)$  and  $W^s(O_\mu)$  start intersecting and, in general (when the map does not possess a certain global symmetry), only one of the stable separatrices of  $O_\mu$ , separatrix  $S_1$ , intersects  $W^u(O_\mu)$  [see Fig. 10(d)].

In the non-orientable case, the Shilnikov funnel formation process is more complicated. We show one of the most common ways when the funnel is formed after the curve  $L_\mu$  undergoes a doubling bifurcation and stable 2-periodic invariant curves  $\hat{L}_\mu^1$  and  $\hat{L}_\mu^2$  become

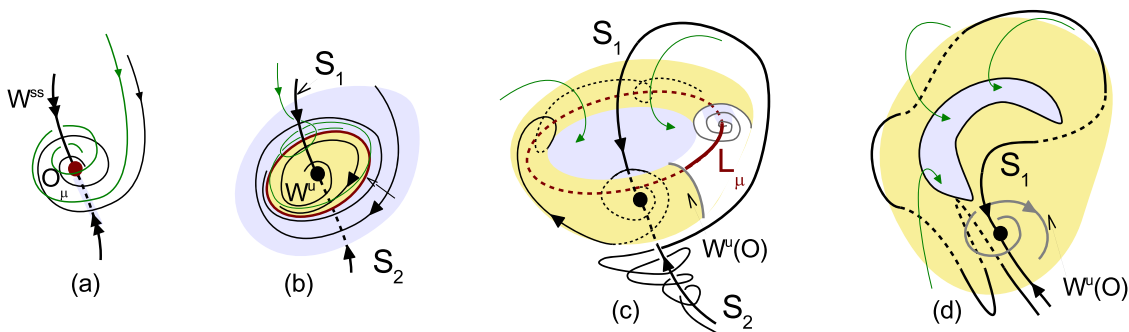


**FIG. 10.** A bifurcation scenario for an orientable discrete Shilnikov attractor: (a)⇒(b) a stable fixed point  $O_\mu$  becomes saddle-focus and a stable closed invariant curve  $L_\mu$  appears under an Andronov–Hopf bifurcation; (b)⇒(c) a Shilnikov funnel near  $L_\mu$  is formed; and (c)⇒(d) an orientable discrete Shilnikov attractor is created.

a focal type. Then, all orbits from the absorbing region are drawn into the two-sided funnel (as a “sac without bottom and lid”). Note that other mechanisms of funnel creation can also exist, see e.g., Ref. 31, but in any case, a non-orientable discrete Shilnikov attractor is two-sided since  $W^u(O_\mu)$  accumulates to  $W^u_{loc}(O_\mu)$  from both sides. In this case,  $W^u(O_\mu)$  intersects both stable separatrices  $S_1$  and  $S_2$  of  $O_\mu$  [see Fig. 8(e)].

#### IV. METHODS FOR FINDING DISCRETE HOMOCLINIC ATTRACTORS

We consider examples of the implementation of the scenarios described in Secs. II and III in the three-dimensional generalized Hénon maps of the form

$$\bar{x} = y, \bar{y} = z, \bar{z} = Bx + Az + Cy + g(y, z), \tag{5}$$

where  $A, B, C$  are parameters [ $B$  is the Jacobian of map (5)],  $g(y, z)$  is a function of the coordinates  $y$  and  $z$  only, and we assume that it vanishes at  $y = z = 0$  together with the first derivatives.

The use of maps of the form (5) is very convenient in experiments with homoclinic attractors in three-dimensional Hénon-like maps. Map (5) appears when we formally shift a fixed point to the origin. Thus, we do not lose any information about the attractors except, perhaps, for the position of the fixed points in the initial map (1) for which it can be an independent problem to find the fixed points. On the other hand, we get more information for the fixed point  $O(0, 0, 0)$  in the case of map (5). Hence, the linear type of the

point  $O$  is easily determined by the characteristic equation

$$\lambda^3 - A\lambda^2 - C\lambda - B = 0. \tag{6}$$

In this case, for any fixed  $B$ , one can construct the so-called saddle chart,<sup>20</sup> where the domains corresponding to different types of the point  $O$  are marked [see Fig. 11(a)]. Since  $-1 < B < 0$ , there exist five different topological types of the hyperbolic point  $O$ , and, accordingly, the bifurcation diagram, see Fig. 11(b) for  $B = -0.5$ , is divided into five domains. One domain corresponds to the case when  $O$  is a sink (stable fixed point), and the other four domains are related to the cases when  $O$  is a saddle point of type (2,1) or (1,2) with different types of orientability on their invariant stable and unstable manifolds. The boundary of these domains are the three bifurcation curves:

- the curve  $L^+$  (corresponds to eigenvalue  $\lambda = 1$ ) with the equation  $C = 1 - B - A$ ;
- the curve  $L^-$  (corresponds to eigenvalue  $\lambda = -1$ ) with the equation  $C = A + B + 1$ ; and
- the curve  $L_\varphi$  (corresponds to eigenvalue  $\lambda_1, \lambda_2 = e^{\pm i\varphi}$ ) with the equation  $C = B^2 - 1 - AB$ ,  $B - 2 \leq A \leq B + 2$ .

Compared to the bifurcation diagram, the saddle chart looks more complicated. The fact is that the saddles differ here in a larger number of characteristics. Specifically, they are distinguished in

- saddles and saddle-foci [the boundary is determined by the relation  $\lambda_1 = \lambda_2$  and it holds in the so-called discriminant curve for Eq. (6)];

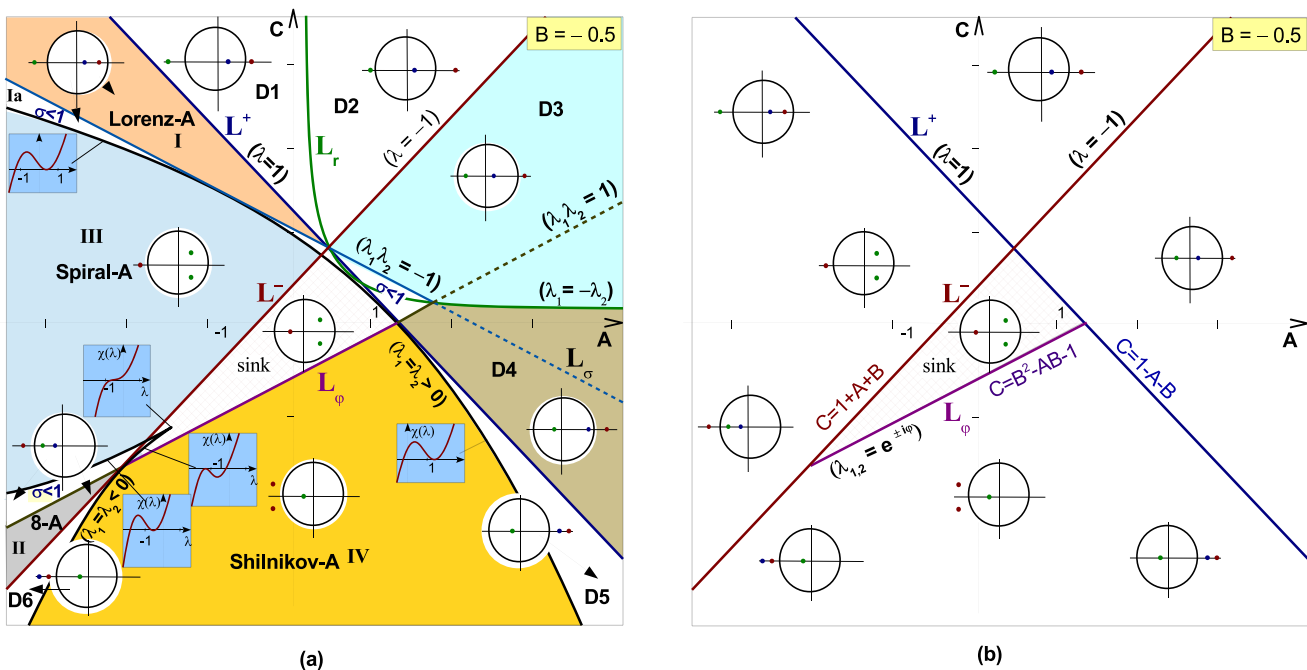


FIG. 11. (a) The saddle chart for the fixed point  $O(0, 0, 0)$  of map (5) with  $B = -0.5$  and (b) the bifurcation diagram for the point  $O$ .

- saddles with  $\sigma < 1$  and  $\sigma > 1$ , where  $\sigma$  is the saddle value  $[|\lambda_1\lambda_2| = 1$  for the boundary that consists of some pieces of the curves  $C = B^2 - 1 - AB$  (when  $\lambda_1\lambda_2 = 1$ ) and  $C = 1 + B^2 + AB$  (when  $\lambda_1\lambda_2 = -1$ ); and
- saddles with different signs of strong stable and strong unstable eigenvalues (the boundary condition  $\lambda_1 = -\lambda_2$  holds on the curve  $AC + B = 0, A > 0$ ).

Note that an analog of the saddle chart in the form of a table was introduced in Ref. 32 for equilibria of three-dimensional flows. Actually, saddle charts were proposed in Ref. 20 for maps of the form (5) with  $0 < B < 1$ . Besides, in Ref. 20, the saddle charts together with the modified diagrams of Lyapunov exponents (the modification consists of the fact that we add to the standard diagram some domains of parameters where the corresponding strange attractor is homoclinic with the fixed point  $O$ ) were effectively used for the numerical search of various homoclinic attractors. The same can be done in the non-orientable case. In the present paper, we show certain results of the corresponding study with the emphasis on demonstration of the scenarios discussed in Secs. II and III by means of the non-orientable maps of the form (5).

### V. EXAMPLES OF SCENARIOS IN THE NON-ORIENTABLE CASE

In this section, we consider concrete examples of the scenarios presented in Secs. II and III in the case of non-orientable

three-dimensional generalized Hénon maps of the form (5). The map (5) always has a fixed point  $O(0,0,0)$  whose type depends only on the parameters  $A, B, C$ . For example, this point is asymptotically stable in the region  $C < 1 - B - A, C < A + B + 1, C > B^2 - 1 - AB$  at  $|B| < 1$ ; see the region “sink” in Fig. 11. We consider the case when the map (5) is non-orientable and dissipative, i.e.,  $-1 < B < 0$ . The orientable case was considered before; see, e.g., Refs. 4, 19, and 20.

The style of our presentations is unified in the following sense. We consider only maps of the form (5), where  $-1 < B < 0$  is fixed,  $A$  and  $C$  are parameters, and  $g(y, z)$  is a given polynomial. For every such family of maps, we construct numerically the Lyapunov exponents diagram in the  $(A, C)$ -parameter plane. This diagram represents a six-colored chart, where different colors correspond to different types of attractors of initial points sufficiently close to the origin  $O(0, 0, 0)$ . The “white” color means that the forward iterations go to infinity; “green” is for a periodic attractor (all the Lyapunov exponents  $\Lambda_1, \Lambda_2, \Lambda_3$  are negative); “cyan” stands for quasiperiodic attractors ( $\Lambda_1 = 0, \Lambda_2 < 0, \Lambda_3 < 0$ ); “yellow” corresponds to chaotic attractors (with  $\Lambda_1 > 0, \Lambda_2 < 0, \Lambda_3 < 0$ ); “deep blue” means hyperchaotic attractors (with  $\Lambda_1 > \Lambda_2 > 0, \Lambda_3 < 0$ ); and “magenta” stands for the case when the corresponding strange attractor contains the point  $O(0, 0, 0)$ , i.e., the chaos is homoclinic. Besides, we also show the saddle charts over the Lyapunov diagrams in order to demonstrate that our attractor is indeed the required homoclinic attractor that contains the fixed point  $O(0, 0, 0)$  with the appropriate set of eigenvalues.

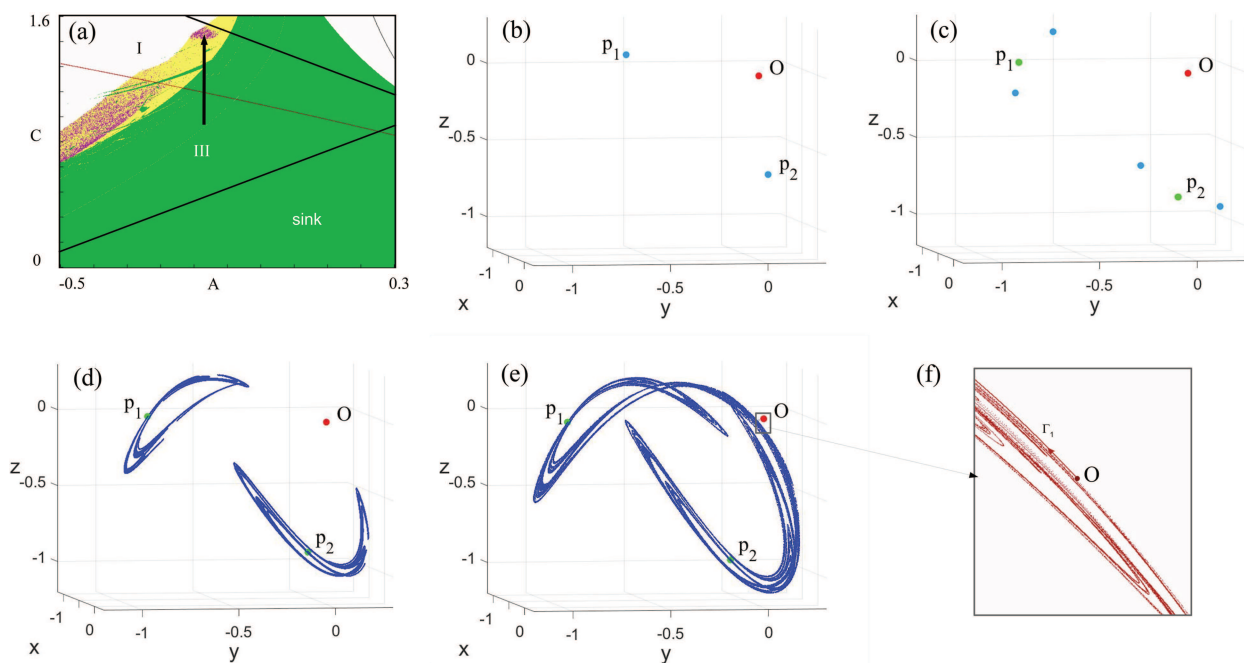


**FIG. 12.** Toward a scenario of appearance of a non-orientable discrete Lorenz-like attractor in map (5) with  $g(y, z) = 1.5yz - 0.54y^3 + 0.54z^3$  and  $B = -0.4$ . (a) A fragment of the Lyapunov diagram. (b)–(e) Stages of the scenario for  $A = -0.13$  when  $C$  changes [black arrow in plot (a)]: (b)  $C = 0.91$ , (c)  $C = 1.23$ , (d)  $C = 1.36$ , and (e)  $C = 1.5$  (Lorenz-like attractor). (f) The unstable separatrix  $\Gamma_1$  near  $O$  in a zoomed rectangle from plot (e), and the separatrix  $\Gamma_2$  behaves symmetrically.

**A. Example of a scenario for a non-orientable discrete Lorenz-like attractor**

In Fig. 12, we show certain stages of the formation of a non-orientable discrete Lorenz-like attractor in the one-parameter family of map (5) with  $g = 1.5yz - 0.54y^3 + 0.54z^3$  and  $B = -0.4$ ,  $A = -0.13$  and  $C$  is a changing parameter. Here, the point  $O(0, 0, 0)$  is asymptotically stable at  $C_0 \approx -0.892 < C < C_1 \approx 0.47$ . At  $C = C_1$ , the point loses stability as a result of a supercritical period doubling bifurcation: it becomes a saddle point and a stable cycle  $(p_1, p_2)$  of period 2 is generated nearby [Fig. 12(b)]. In turn, when  $C$  changes, the cycle  $(p_1, p_2)$  loses stability as a result of a period doubling bifurcation [Fig. 12(c)].

This and subsequent bifurcations can lead<sup>4</sup> to the appearance of a two-component discrete attractors, which contain the cycle  $(p_1, p_2)$ . Such an attractor is shown in Fig. 12(d). With further change of  $C$ , these two components of the attractor merge into a one-component discrete Lorenz-like attractor, which contains the fixed point  $O$  [Fig. 12(e)]. We note that the eigenvalues  $\lambda_1 = -1.403$ ,  $\lambda_2 = 0.982$ ,  $\lambda_3 = 0.290$  of  $O$  satisfy conditions (2). In Fig. 12(f), for  $C = 1.5$ , the unstable separatrix  $\Gamma_1$  near  $O$  is plotted, and the separatrix  $\Gamma_2$  behaves symmetrically. This is quite consistent with the theoretical constructions from Sec. II A.

**B. Example of a scenario for a non-orientable discrete figure-8 attractor**

In Fig. 13, we display the stages of the appearance of a non-orientable figure-8 attractor in the one-parameter

family of map (5) with  $g = y^2 + 10yz + 1.5z^2 + 2z^3$ ,  $B = -0.5$ ,  $C = (2A - 1)/3$  and  $A$  varies. In this way, the point  $O(0, 0, 0)$  loses stability as a result of a period doubling bifurcation at  $A = -2.5$ : the point  $O$  becomes a saddle point of type (2,1) and a stable orbit  $(p_1, p_2)$  of period 2 appears in its neighborhood [Fig. 13(b)]. When we decrease  $A$  further, the cycle  $(p_1, p_2)$  loses stability as a result of an Andronov–Hopf bifurcation after which the attractor is a closed invariant curve of period 2, Fig. 13(c); this invariant curve, in turn, is destroyed according to one of the Afraimovich–Shilnikov scenarios,<sup>9</sup> and, first, a two-component strange attractor of the “torus-chaos” type is formed, and, then, a non-orientable discrete figure-8 attractor emerges, which contains the point  $O$ , Fig. 13(d). In Fig. 13(e), we also illustrate the unstable separatrix  $\Gamma_1$  for  $A = -2.599$  (the separatrix  $\Gamma_2$  is located symmetrically). We point out that the eigenvalues  $\lambda_1 = -1.351$ ,  $\lambda_2 = -0.485$ ,  $\lambda_3 = -0.762$  of the point  $O$  satisfy conditions (3).

**C. Examples of scenarios for non-orientable discrete spiral figure-8 attractors**

In Fig. 14, we present the stages of the appearance of a non-orientable spiral figure-8 attractor in the one-parameter family of map (5) with  $g(y, z) = -1.5yz - y^3 + 1.45z^3$  for  $B = -0.8$ ,  $C = -2.37$  and  $A$  changes. The point  $O(0, 0, 0)$  is asymptotically stable for  $A^* = -2.57 < A < -2.5125$  [Fig. 14(b)]. When  $A = A^*$ , the point loses stability as a result of a period doubling bifurcation: the point becomes a saddle point (whose eigenvalues satisfy

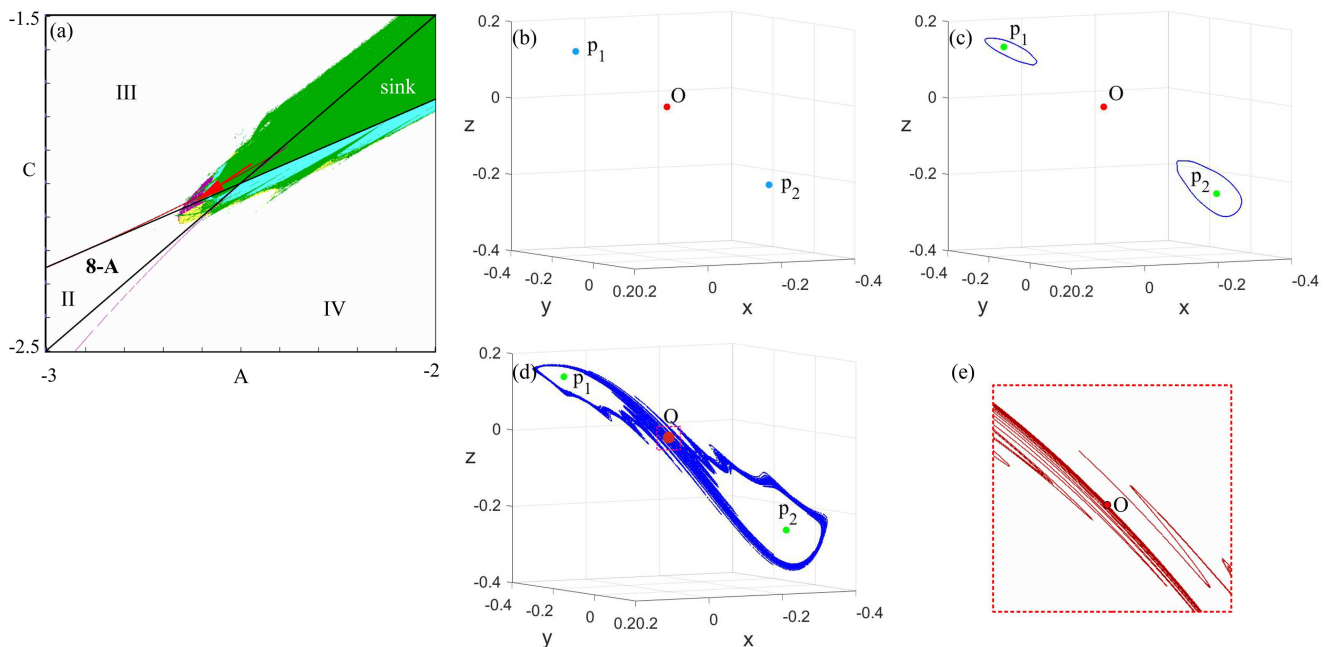


**FIG. 13.** Toward a scenario of the appearance of a non-orientable figure-8 attractor in map (5) with  $g(y, z) = y^2 + 1.5z^2 + 10yz + 2z^3$  and  $B = -0.5$ . (a) A fragment of the Lyapunov diagram. (b)–(d) Stages of the scenario for  $C = \frac{2}{3}A - \frac{1}{3} + 0.01$  when  $A$  changes [red arrow in plot (a)]: (b)  $A = -2.59$ , (c)  $A = -2.585$ , and (d)  $A = -2.599$  (the figure-8 attractor). (e) A zoomed fragment of a neighborhood of  $O$  with pieces of the unstable separatrix  $\Gamma_1$ .

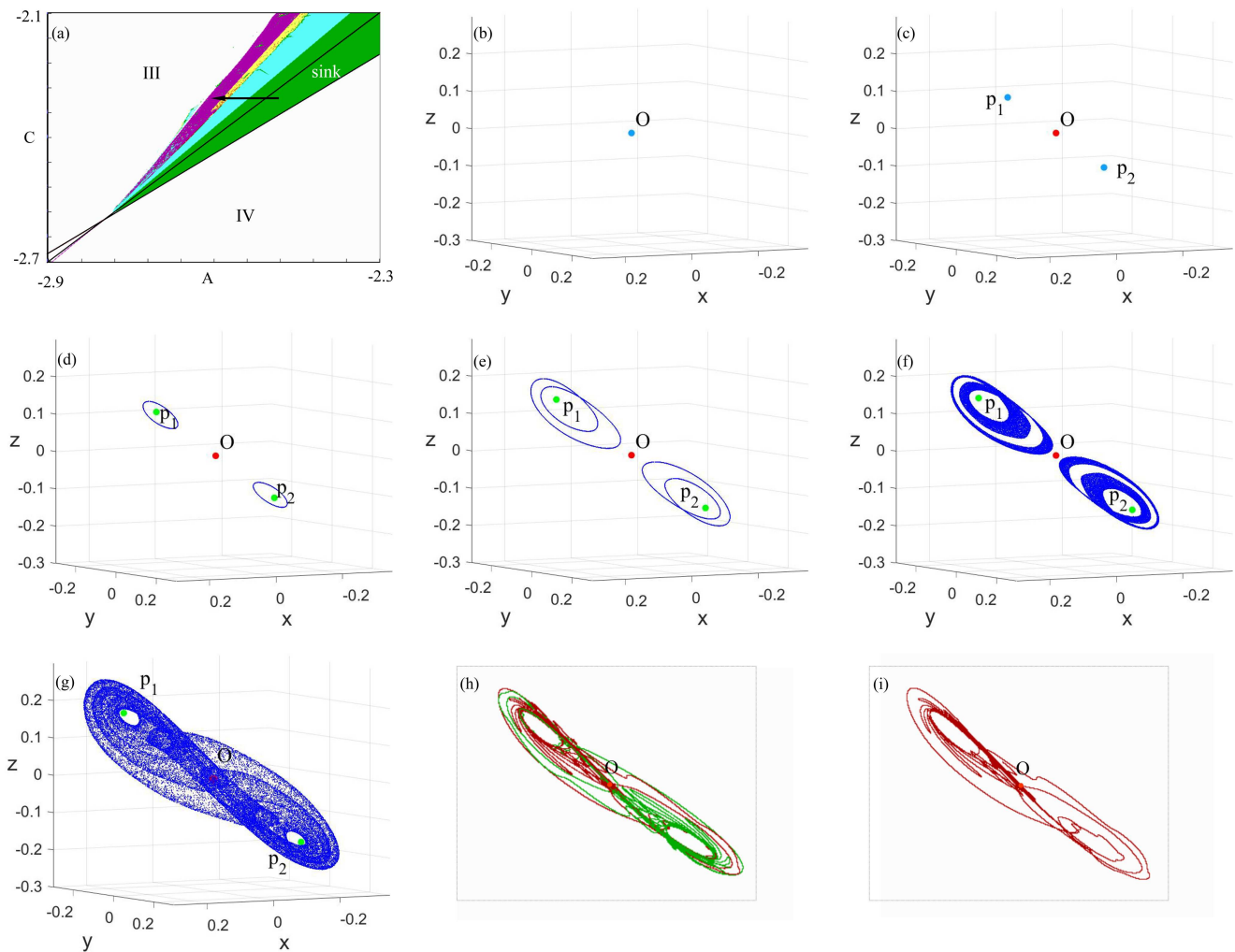


**FIG. 14.** Toward a scenario of the appearance of a non-orientable discrete spiral figure-8 attractor in map (5) with  $g(y, z) = -1.5yz - y^3 + 1.45z^3$  and  $B = -0.8$ . (a) A fragment of the Lyapunov diagram. (b)–(g) Stages of the scenario for  $C = -2.37$  when  $A$  changes [black arrow in plot (a)]; (b)  $A = -2.56$ , (c)  $A = -2.59$ , (d)  $A = -2.60$ , (e)  $A = -2.618$ , (f)  $A = -2.621$ , and (g)  $A = -2.638$  (the spiral figure-8 attractor). (h)–(i) The unstable separatrices  $\Gamma_1$  (in red) and  $\Gamma_2$  (in green) of  $O$  for  $A = -2.638$ .

$\lambda_1 < -1, \lambda_2, \lambda_3 = \rho e^{\pm i\omega}$ , where  $0 < \rho < 1, 0 < \omega < \pi$ ), and a stable cycle  $(p_1, p_2)$  of period 2 is generated around [Fig. 14(c)]. When  $A$  decreases further, the cycle  $(p_1, p_2)$  loses stability as a result of an Andronov–Hopf bifurcation when the closed invariant curve of period 2 becomes attracting [Fig. 14(d)]. Furthermore, this curve undergoes a series of bifurcations; in particular, in Fig. 14(e), the result of a doubling bifurcation is shown, which leads to a two-component strange attractor of the “torus-chaos” type that appears [Fig. 14(f)]. Then, this attractor is transformed into a non-orientable discrete spiral figure-8 attractor, which contains the point  $O$  [Fig. 14(g)]. In Figs. 14(h) and 14(i), we display the unstable manifold of the saddle point  $O$  for  $A = -2.638$ , which consists of two separatrices  $\Gamma_1$  in red and  $\Gamma_2$  in green.

In Fig. 15, we show a variant of the scenario when passing close to the 1:4 resonance when the point  $O$  has eigenvalues  $\lambda_1 < -1, \lambda_2, \lambda_3 = \lambda e^{\pm i\varphi}$ , where  $0 < \lambda < 1$  is close to 1 and  $\varphi$  is close to  $\pi/2$ . We follow this scenario in the one-parameter family of map (5) with  $g(y, z) = -1.5yz - y^3 + 1.45z^3$  for  $B = -0.8, A = -1.1$ , and  $C$  varies. After a period doubling bifurcation (for  $C = -0.9$ ), the attractor becomes a 2-periodic orbit  $(p_1, p_2)$ , Fig. 15(b), and after a second period doubling bifurcation, it is a 4-periodic orbit, Fig. 15(c). Then, the 4-periodic orbit undergoes an Andronov–Hopf bifurcation and the attractor becomes a 4-component closed invariant curve [Fig. 15(d)]. Then, a 2-periodic Lorenz-like attractor containing the saddle 2-periodic orbit  $(p_1, p_2)$  is created [Fig. 15(e)]. Finally, this two-component attractor collides with the point  $O$ , and a specific spiral figure-8 attractor is formed, which contains both the

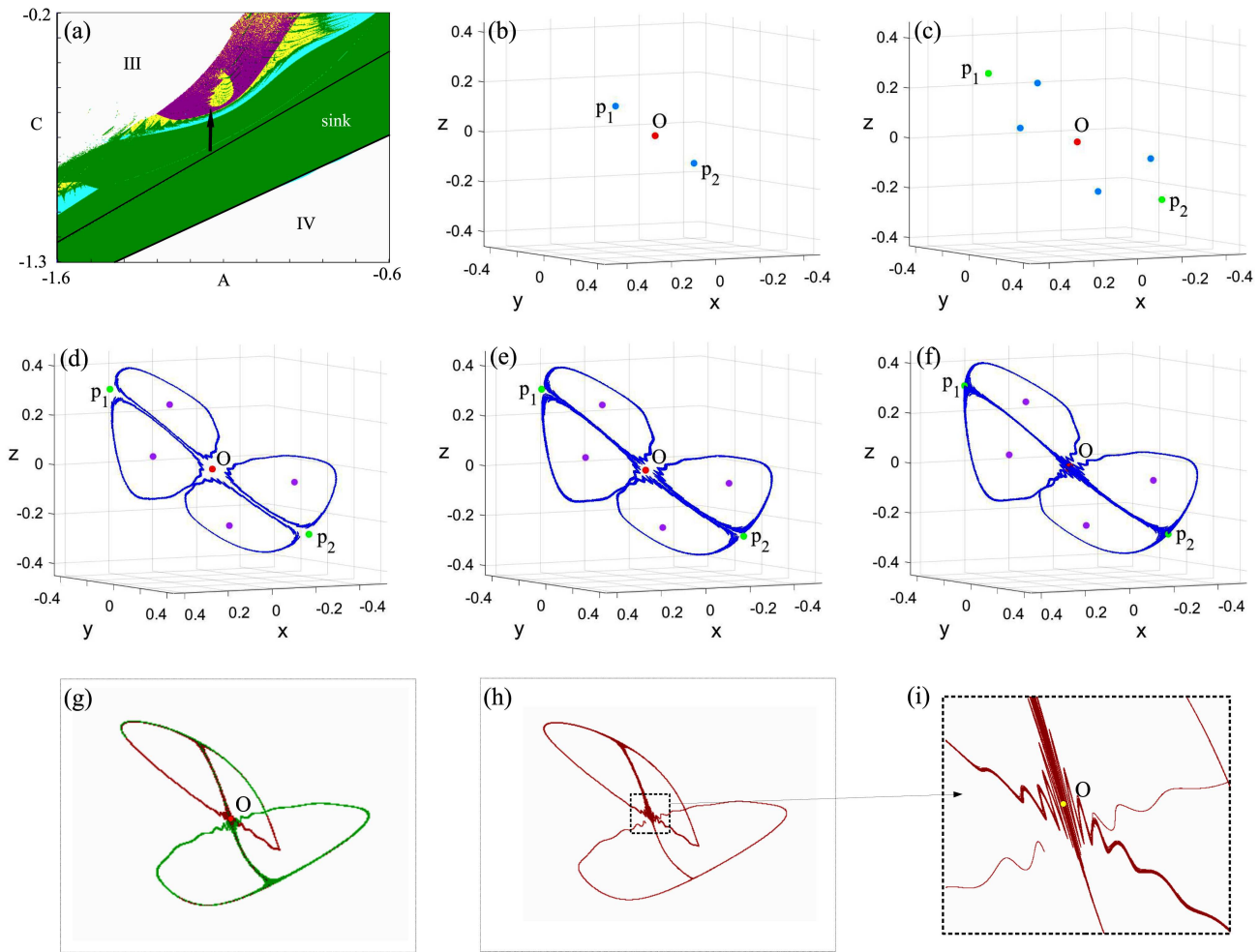


**FIG. 15.** Toward a scenario of the appearance of a non-orientable discrete spiral figure-8 attractor in map (5) with  $g(y, z) = -1.5yz - y^3 + 1.45z^3$  and  $B = -0.8$ . (a) A fragment of the Lyapunov diagram. (b)–(f) Stages of the scenario for  $A = -1.1$  and changing  $C$  [black arrow in plot (a)]: (b)  $C = -0.87$ , (c)  $C = -0.75$ , (d)  $C = -0.69586$ , (e)  $C = -0.694$ , and (f)  $C = -0.69$  (the spiral figure-8 attractor). (g)–(i) The unstable separatrices of  $O$  are shown for  $C = -0.69$ : (g) both separatrices  $\Gamma_1$  (in red) and  $\Gamma_2$  (in green) and (h) one separatrix  $\Gamma_1$ , which is also displayed in a zoomed fragment near  $O$  in plot (i).

saddle-focus fixed point  $O$  and the 2-periodic orbit  $(p_1, p_2)$  in the boundary [Fig. 15(f)]. In Figs. 15(g)–15(i), the unstable manifold of the saddle point  $O$  is displayed for  $C = -0.69$  along with the separatrices  $\Gamma_1$  (in red) and  $\Gamma_2$  (in green). We note also that the point  $O$  has eigenvalues  $\lambda_1 = -1.121, \lambda_{2,3} = 0.01 \pm 0.84i$ .

#### D. Example of a scenario for a non-orientable discrete Shilnikov attractor

In Fig. 16, we demonstrate the stages of the appearance of a non-orientable discrete Shilnikov attractor in the one-parameter family of map (5) with  $g(y, z) = -y^2 + yz$  for  $B = -0.7$ ,  $A = -2.446$ , and  $C$  is a parameter whose range of values is shown by the red arrow in the Lyapunov diagram [Fig. 16(a)].

After a supercritical Andronov–Hopf bifurcation (for  $A = -2.446$ ,  $C = -2.222$ ), the attractor is a stable closed invariant curve  $L$  [Figs. 16(b) and 16(c)]. When we decrease  $A$ , first,  $L$  undergoes a doubling bifurcation, after which a 2-periodic closed invariant curve  $(L_1, L_2)$ , where  $T(L_1) = L_2$  and  $T(L_2) = L_1$ , becomes the attractor [Fig. 16(d)]. Then, this 2-periodic curve becomes non-smooth, Fig. 16(e), is destroyed, and is transformed into a torus-chaos that can look as a chaotic resonance, Fig. 16(f), or as a developed torus-chaos, Fig. 16(g). Finally, a non-orientable discrete Shilnikov attractor appears [Fig. 16(h)]. In Fig. 16(i), the stable manifold of the saddle point  $O$  is shown for  $C = -2.4$ . Note also that other examples of non-orientable discrete Shilnikov attractors, including hyperchaotic ones, in non-orientable generalized Hénon maps were found in Ref. 31 where a two-parameter



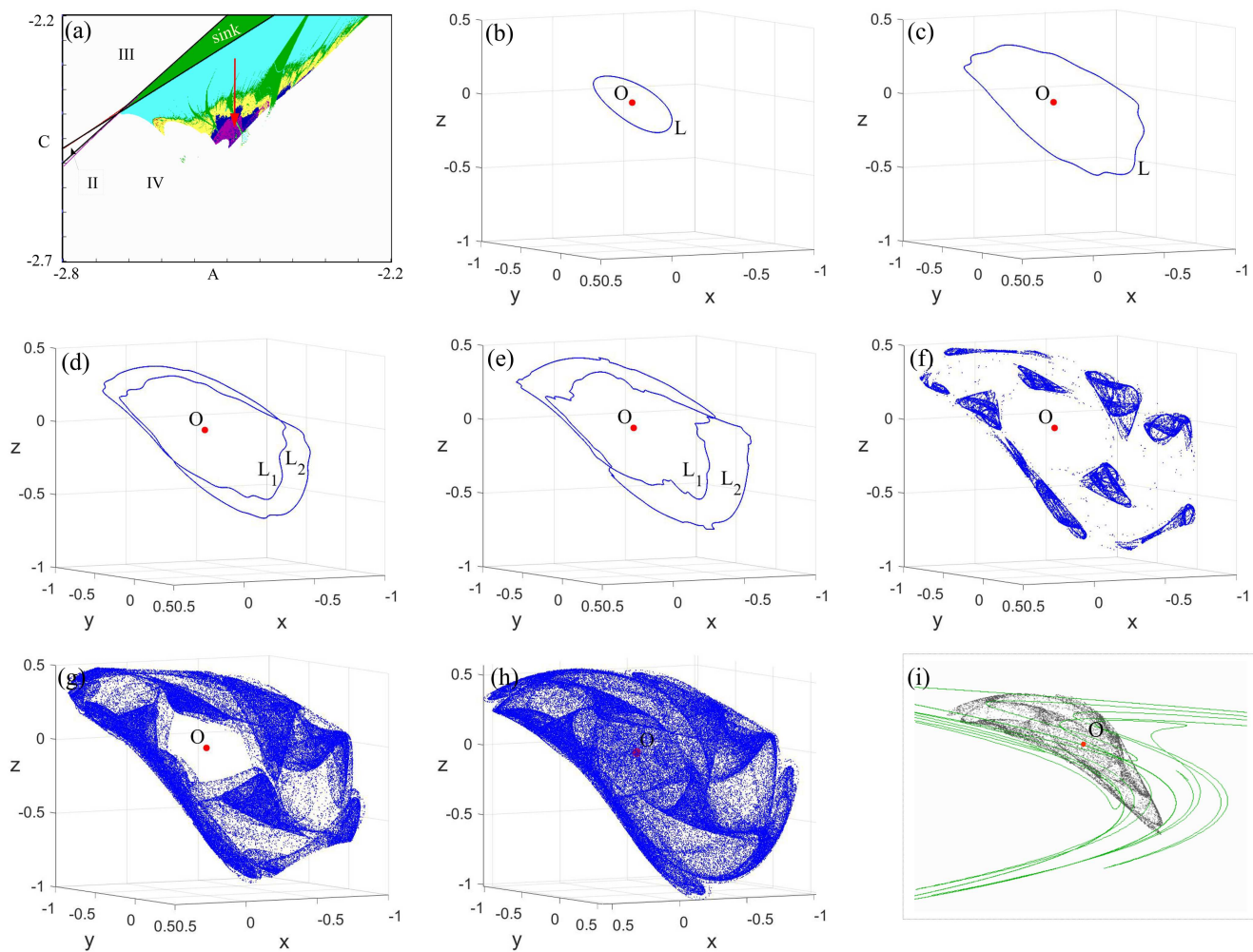


**FIG. 16.** Toward a scenario of the appearance of a non-orientable discrete Shilnikov attractor in map (5) with  $g(y, z) = -y^2 + yz$  and  $B = -0.7$ . (a) A fragment of the Lyapunov diagram. (b)–(g) Stages of the scenario for  $A = -2.446$  when  $C$  changes [red arrow in plot (a)]: (b)  $C = -2.24$ , (c)  $C = -2.31$ , (d)  $C = -2.325$ , (e)  $C = -2.34$ , (f)  $C = -2.38$ , (g)  $C = -2.39$ , and (h)  $C = -2.4$  (the Shilnikov attractor). (i) The stable manifold of  $O$  for  $C = -2.4$ .

bifurcation analysis related to their appearance was carried out as well.

### VI. FINAL REMARKS AND OPEN PROBLEMS

Scenarios of chaos development related to the appearance of discrete homoclinic attractors in orientable three-dimensional maps were proposed in Ref. 4. Afterward, the corresponding theory and methods of searching for such attractors were developed in Refs. 12 and 18–20. The non-orientable case has been much less studied, but as shown in the present paper, see also Ref. 33, it is also very interesting and promising. However, a lot of new questions arise here. In particular, this concerns the theory of pseudohyperbolicity of non-orientable homoclinic attractors. We have not found yet examples of such attractors (with fixed points). In any case, we do

not see any fundamental obstacles that the non-orientable Lorenz-like and figure-8 attractors could not be pseudohyperbolic. In the non-orientable case, such (pseudohyperbolic) attractors also exist, but so far, this is known only for attractors of period 2, whose examples are shown in Fig. 17. In particular, as shown in Ref. 12, such pseudohyperbolic attractors can be 2-periodic Lorenz-like attractors, as in Fig. 17(a). These attractors are also interesting because their crises lead to the appearance of attractors (including pseudohyperbolic ones) of new types, whose flow analogs were not known even for the three-dimensional case. We refer the reader to Ref. 12 where the related problems have been studied in detail.

The same can be said about our non-orientable attractors. For example, a non-orientable Shilnikov attractor may have an analog in the case of a three-dimensional flow with symmetry. It differs from the classical Shilnikov attractor by the fact that both stable

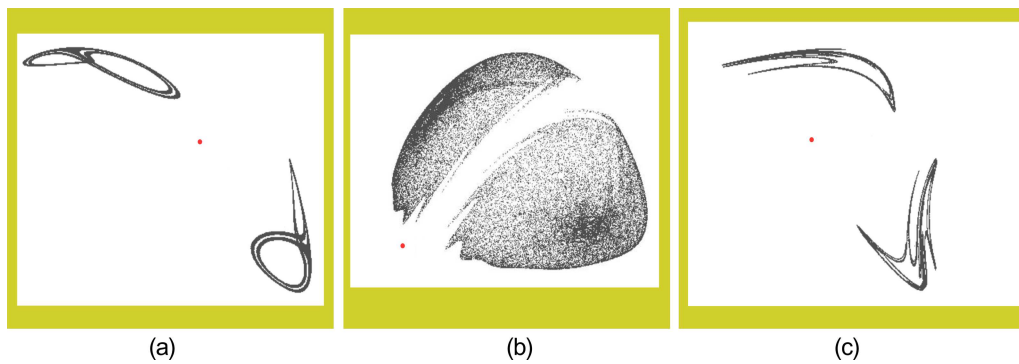


**FIG. 17.** Examples of 2-periodic homoclinic attractors in three-dimensional non-orientable Hénon-like maps: (a) Lorenz-like attractor, (b) Shilnikov-like attractor, and (c) figure-8 attractor.

separatrices of a saddle-focus can enter into the attractor, forming homoclinic figure-8 loops of the equilibrium state. As far as we know, such spiral attractors have not been observed yet in flows.

## ACKNOWLEDGMENTS

The authors thank S. Gonchenko and D. Turaev for fruitful discussions and remarks. This work was carried out in the framework of Grant No. 20-71-00079 of the RSciF. Section II was supported by Grant No. 19-11-00280 of the RSciF, Sec. II C by RFBR Grant No. 19-01-00607, and Sec. III C by RFBR Grant No. 18-29-10081. The authors are partially supported (numerical results of Sec. V) by the Laboratory of Dynamical Systems and Applications NRU HSE of the Ministry of Science and Higher Education of the RF grant [Ag. No. 075-15-2019-1931]. E.A.S. thanks the Theoretical Physics and Mathematics Advancement Foundation “BASIS.” M.S.G. was partially supported by the Juan de la Cierva-Incorporación fellowship (No. IJCI-2016-29071) and the Spanish grant (No. PGC2018-098676-B-I00) (AEI/FEDER/UE).

## DATA AVAILABILITY

The data that support the findings of this study are available from the corresponding author upon reasonable request.

## REFERENCES

- <sup>1</sup>E. Lorenz, “Deterministic nonperiodic flow,” *J. Atmos. Sci.* **20**, 130–141 (1963).
- <sup>2</sup>M. Hénon, “A two-dimensional mapping with a strange attractor,” in *The Theory of Chaotic Attractors* (Springer, New York, 1976), pp. 94–102.
- <sup>3</sup>L. P. Shilnikov, “The theory of bifurcations and turbulence. I,” in *Methods of Qualitative Theory of Differential Equations* (Gorky, 1986), pp. 150–163 (in Russian) [English translation in *Selecta Math. Sov.* **10**(1), 43–53 (1991)].
- <sup>4</sup>A. S. Gonchenko, S. V. Gonchenko, and L. P. Shilnikov, “Towards scenarios of chaos appearance in three-dimensional maps,” *Rus. J. Nonlin. Dyn.* **8**, 3–28 (2012) (in Russian).
- <sup>5</sup>L. D. Landau, “On the problem of turbulence,” *Dokl. Akad. Nauk SSSR* **44**, 339–342 (1944) (in Russian).
- <sup>6</sup>E. Hopf, “A mathematical example displaying the features of turbulence,” *Commun. Pure Appl. Math.* **1**, 303–322 (1948).
- <sup>7</sup>D. Ruelle and F. Takens, “On the nature of turbulence,” *Commun. Math. Phys.* **20**(3), 167–192 (1971).

- <sup>8</sup>M. J. Feigenbaum, “Quantitative universality for a class of nonlinear transformations,” *J. Stat. Phys.* **19**, 25–52 (1978).
- <sup>9</sup>V. S. Afraimovich and L. P. Shilnikov, “Invariant two-dimensional tori, their breakdown and stochasticity,” in *Methods of Qualitative Theory of Differential Equations* (Gorky, 1983), pp. 3–26 [English translation in *Am. Math. Soc. Transl., Ser. 2* **149**, 201–212 (1991)].
- <sup>10</sup>Z. Galias and W. Tucker, “Is the Hénon attractor chaotic?,” *Chaos* **25**, 033102 (2015).
- <sup>11</sup>A. S. Gonchenko, S. V. Gonchenko, A. O. Kazakov, and A. D. Kozlov, “Elements of contemporary theory of dynamical chaos: A tutorial. Part I. Pseudohyperbolic attractors,” *Int. J. Bifurcat. Chaos Appl. Sci. Eng.* **28**, 1830036 (2018).
- <sup>12</sup>S. V. Gonchenko, A. S. Gonchenko, A. O. Kazakov, and E. A. Samylnina, “On discrete Lorenz-like attractors,” *Chaos* **31**, 023117 (2021).
- <sup>13</sup>A. S. Gonchenko, S. V. Gonchenko, A. O. Kazakov, A. D. Kozlov, and Y. V. Bakhanova, “Mathematical theory of dynamic chaos and its applications: Review Part 2. Spiral chaos of three-dimensional flows,” *Izv. Vuz. Appl. Nonlin. Dyn.* **27**, 7–52 (2019).
- <sup>14</sup>V. S. Afraimovich, V. V. Bykov, and L. P. Shilnikov, “The origin and structure of the Lorenz attractor,” *Sov. Phys. Dokl.* **22**, 253–255 (1977).
- <sup>15</sup>J. Marsden, “Attempts to relate the Navier-Stokes equations to turbulence,” in *Turbulence Seminar*, Lecture Notes in Mathematics Vol. 615, edited by P. Bernard and T. Ratiu (Springer-Verlag, New York, 1977).
- <sup>16</sup>L. P. Shilnikov, “Bifurcation theory and the Lorenz model,” in *The Hopf Bifurcation and Its Applications* (in Russian) [Translated to Russian: J. Marsden and M. MacKraken, “Bifurcation of birth of cycle and its applications,” *M.:Mir* 317–336 (1980)].
- <sup>17</sup>S. Gonchenko, I. Ovsyannikov, C. Simo, and D. Turaev, “Three-dimensional Hénon-like maps and wild Lorenz-like attractors,” *Int. J. Bifurcat. Chaos Appl. Sci. Eng.* **15**, 3493–3508 (2005).
- <sup>18</sup>S. V. Gonchenko, A. S. Gonchenko, I. I. Ovsyannikov, and D. V. Turaev, “Examples of Lorenz-like attractors in Hénon-like maps,” *Math. Model. Nat. Phen.* **8**, 48–70 (2013).
- <sup>19</sup>A. S. Gonchenko, S. V. Gonchenko, A. O. Kazakov, and D. Turaev, “Simple scenarios of onset of chaos in three-dimensional maps,” *Int. J. Bifurcat. Chaos Appl. Sci. Eng.* **24**, 25 (2014).
- <sup>20</sup>A. Gonchenko and S. Gonchenko, “Variety of strange pseudohyperbolic attractors in three-dimensional generalized Hénon maps,” *Physica D* **337**, 43–57 (2016).
- <sup>21</sup>A. V. Borisov, A. O. Kazakov, and I. R. Sataev, “The reversal and chaotic attractor in the nonholonomic model of Chaplygin’s top,” *Regul. Chaotic Dyn.* **19**, 718–733 (2014).
- <sup>22</sup>A. V. Borisov, A. O. Kazakov, and I. R. Sataev, “Spiral chaos in the nonholonomic model of a Chaplygin top,” *Regul. Chaotic Dyn.* **21**, 939–954 (2016).
- <sup>23</sup>S. V. Gonchenko, A. S. Gonchenko, and A. O. Kazakov, “Richness of chaotic dynamics in nonholonomic models of a Celtic stone,” *Regul. Chaotic Dyn.* **15**, 521–538 (2013).

- <sup>24</sup>A. Gonchenko and E. Samylna, “On the region of existence of a discrete Lorenz attractor in the nonholonomic model of a Celtic stone,” *Radiophys. Quantum Electron.* **62**, 369–384 (2019).
- <sup>25</sup>A. Chenciner and G. Iooss, “Bifurcations de tores invariants,” *Arch. Ration. Mech. Anal.* **1249**, 109–198 (1979).
- <sup>26</sup>A. L. Shilnikov, “On bifurcations of the Lorenz attractor in the Shimuizu-Morioka model,” *Physica D* **62**, 338–346 (1993).
- <sup>27</sup>V. S. Afraimovich, V. V. Bykov, and L. P. Shilnikov, “On attracting structurally unstable limit sets of Lorenz attractor type,” *Trans. Mosc. Math. Soc.* **44**, 153–216 (1982).
- <sup>28</sup>D. V. Turaev and L. P. Shilnikov, “Pseudo-hyperbolicity and the problem on periodic perturbations of Lorenz-like attractors,” *Dokl. Math.* **77**(1), 17–21 (2008).
- <sup>29</sup>H. W. Broer, G. B. Huitema, F. Takens, and B. L. J. Braaksma, “Unfoldings and bifurcations of quasiperiodic tori,” *Mem. Am. Math. Soc.* **83**, 421 (1990).
- <sup>30</sup>R. Vitolo, H. W. Broer, and C. Simó, “Quasi-periodic bifurcations of invariant circles in low-dimensional dissipative dynamical systems,” *Regul. Chaotic Dyn.* **16**, 154–184 (2011).
- <sup>31</sup>E. Karatetskaia, A. Shykhmamedov, and A. Kazakov, “Shilnikov attractors in three-dimensional orientation-reversing maps,” *Chaos* **31**, 011102 (2021).
- <sup>32</sup>L. P. Shilnikov, A. L. Shilnikov, D. V. Turaev, and L. O. Chua, *Methods of Qualitative Theory in Nonlinear Dynamics. Part I* (World Scientific, 1998); Part II (World Scientific, 2001).
- <sup>33</sup>A. S. Gonchenko and A. D. Kozlov, “On scenarios of chaos appearance in three-dimensional nonorientable maps (in Russian),” *Zhurnal SVMO* **18**, 17–29 (2016).